

Review

The Applications of Metallacycles and Metallacages

Changfeng Yin ¹, Jiaxing Du ¹, Bogdan Olenyuk ², Peter J. Stang ^{3,*} and Yan Sun ^{1,*}

¹ Key Laboratory for Special Functional Materials of Ministry of Education, National & Local Joint Engineering Research Center for High-Efficiency Display and Lighting Technology, School of Materials Science and Engineering, Collaborative Innovation Center of Nano Functional Materials and Applications, Henan University, Kaifeng 475004, China

² Proteogenomics Research Institute for Systems Medicine, La Jolla, CA 92037, USA

³ Department of Chemistry, University of Utah, Salt Lake City, UT 84112, USA

* Correspondence: stang@chem.utah.edu (P.J.S.); elaine.sun@utah.edu (Y.S.)

Abstract: Metallacycles and metallacages constitute a class of coordination compounds composed of metal ions and organic ligands. Because of their precise stoichiometry, the flexibility and viability of design, metallacycles and metallacages have attracted considerable attention as supramolecular assemblies. Various two-dimensional polygons, three-dimensional polyhedra, and other nanoscale materials have been constructed and applied. The highly diverse structures, sizes, and shapes endow metallacycles and metallacages with unique physical and chemical properties and make them suitable for various applications such as encapsulation, separation, catalysis, and biological science. Herein, we review the recent developments in various metallacycles and metallacages in different fields. The text highlights biomedical applications involving molecular recognition and binding, antibacterial activity, and especially cancer diagnosis and treatment, including imaging, chemotherapy, PDT, and PTT.

Keywords: metallacycles; metallacages; biomedical applications; anticancer



Citation: Yin, C.; Du, J.; Olenyuk, B.; Stang, P.J.; Sun, Y. The Applications of Metallacycles and Metallacages. *Inorganics* **2023**, *11*, 54. <https://doi.org/10.3390/inorganics11020054>

Academic Editors: Rainer Winter and Bruno Therrien

Received: 21 December 2022

Revised: 19 January 2023

Accepted: 20 January 2023

Published: 22 January 2023



Copyright: © 2023 by the authors. Licensee MDPI, Basel, Switzerland. This article is an open access article distributed under the terms and conditions of the Creative Commons Attribution (CC BY) license (<https://creativecommons.org/licenses/by/4.0/>).

1. Introduction

Metallacycles and metallacages are members of a class of metal organic complexes (MOCs) that are accessed through coordination-driven self-assembly [1–4]. The bonding between metal and ligand, which serves as the driving force for assembly, promotes the formation of two-dimensional polygons, three-dimensional polyhedra, and other nanoscale materials [5–7]. Different kinds of organic ligands can be used as building blocks to prepare metal organic complexes, such as bis-pyridyl, ter-pyridyl, and heterotopic ligands. Recently, researchers have prepared many types of metallacycles and metallacages with different shapes and sizes, such as triangles [8–10], rectangles [11], hexagons [12–14], trigonal prisms [15], hexagonal prisms [16,17], and cubes [18,19], in which the overall performance can be designed to achieve interesting properties and functions through the interaction between metal centers and ligands. For example, tetraphenylethylene (TPE), boron-dipyrromethene (BODIPY), and porphyrin have been employed to endow fluorescent and imaging abilities. Significant progress has been made in the development of Pt- and Pd-based metallacycles and metallacages due to the efforts of Stang, Fujita, and other groups. In addition, other metal centers, such as Ru [20–22], Fe [23,24], Ir [25,26], Zn [27], Ni [28], and Co [29,30], can also be introduced into various metallacycles and metallacages.

Metallacycles and metallacages have attracted considerable scientific interest because of their advantages of well-organized architectures and tunable sizes and their unique structure and excellent application prospects [13], including guest recognition [31], encapsulation [32], separation [33], catalysis [29], sensing [34], drug delivery [18], etc. With increased structural complexity and novel designs of metal acceptors and ligand donors, biological studies related to metallacycles and metallacages have been widely carried out,

with these complexes being used as anticancer agents, drug carriers, and photosensitizers in chemotherapeutic or phototherapeutic treatment. Multiple functional systems involving metallacycles and metallacages can also be constructed to reduce biological toxicity and side effects and enhance enrichment in tumors via active or passive target transport; this strategy is the same as that used for nanodrug delivery systems [35,36].

In this review, a number of metallacycles and metallacages based on different metal centers are introduced. More importantly, we present recent developments in different fields, with a focus on biological applications.

2. Applications of Metallacycles and Metallacages

2.1. Encapsulation and Separation

With well-defined shapes and cavities, host-guest inclusion complexes can be formed through weak interactions, which have attracted the attention of scientists in the field of supramolecular chemistry, and numerous systems have been developed to investigate the encapsulation and separation of various guests. To realize the recognition process, it is necessary to maintain a relatively short distance between the guest and the host molecule, which requires matching their size and shape. In this regard, metallacycles and metallacages formed by the self-assembly of metal ions and organic ligands may provide obvious advantages for tunable structures and sizes.

The anion encapsulation and separation ability of metallacages open up future applications in extraction and recovery. Nitschke and coworkers reported a Co_{12}L_6 cuboctahedron metallacage M1 (Figure 1a) that is able to cooperatively bind neutral guests and anions [37]. They also prepared an azaphosphatrane-functionalized Fe_4L_4 tetrahedron metallacage M2 and investigated the hydrogen-bond donating ability of $^+\text{P-H}$ through anion recognition [38]. Based on the strong electrostatic driving force, the affinity of the hydrogen bond donor, and its good solubility and flexibility, M2 can encapsulate anions within the volume range of 35–219 \AA^3 inside the cavity. In subsequent work, researchers reported that M2 was able to extract equimolar amounts of ReO_4^- and TcO_4^- from water into nitromethane (Figure 1b) [39]. This work demonstrated the feasibility of metallacages for two-phase extraction. Fujita's group constructed a trinuclear Ir(III)-based metallacage M3 that contained three adaptive binding pockets on its rim and was capable of recognizing anions. Anions were recognized and bound on the rim instead of being encapsulated into the cavity [25].

It is necessary to develop selective confinement technology for rare earth metal ions. Fujita and coworkers reported a cationic octahedral metallacage M4, which consisted of Pd^{II} coordination blocks and tridentate electron-deficient ligands. The cavity of M4 can selectively isolate rare earth metal ions (La^{3+} - Eu^{3+}) under the action of tripodal anionic caps in a solution state, in which the hydrates are recognized in the isolated space [40]. Benefiting from the cap-like counteranions in the cage's portals, early lanthanoid(III) ions could be selectively encapsulated into the metallacages from a mixture of two different metal ions via electrostatic interactions, as confirmed by the visualization of competitive dye inclusion.

The cavities of metallacages have also been used for selective molecular separation. Systems have been established to recognize different kinds of guest molecules, including reactive molecules and intermediates. Due to the quite small windows, rhombic dodecahedral metallacages can enclose small molecules. Li described that the Ni-imidazolate $\text{Ni}_{14}\text{L}_{24}$ metallacage M5 was able to selectively encapsulate CO_2 molecules among several small gas molecules in both solution and the solid state (Figure 1c) [41]. The CO_2 molecules could be encapsulated and imprisoned into the cavities under relatively high pressure or supercritical conditions but could not escape from the cages freely. Yuan generated homochiral Zn_3L_2 metallacage M6 and explored its application in gas chromatographic separations [33]. The manufactured capillary column coated by M6 showed noteworthy chirality recognition and separation of multiple analytes, including polycyclic aromatic hydrocarbons, n-alkanes, racemates, and positional isomers. By stabilizing twisted amides into the cavity of Pd (II) or Pt (II) octahedral metallacages, the reactivity toward hydrolysis under basic conditions

through the noncovalent trapping of reactive guests was enhanced by Fujita [42]. As shown in Figure 1d, the planar conformation of the amine group was distorted from planar to twisted due to spatial constraints. As a result, the hydrolysis of amides was obviously accelerated upon encapsulation. Recently, they fixed a 2-biphenylacetylene moiety into the confined cavity of M4, in which a regioselective spirocyclization was performed in the presence of an electrophile [43]. In addition, a semiflexible metallacage M7 with a double wall was also constructed [44], which was able to recognize and encapsulate tetrachloromethane in $\text{CD}_3\text{CN}/\text{D}_2\text{O}$ solution through the adaptive portal and expansionary cavity.

Larger molecules, such as fullerene [32,45–47] and proteins with a smaller size than the inner diameter [48], have also been used to explore the encapsulation capability of metallacages. A cubic metallacage M8 with electron-deficient walls was reported [49]. It can selectively bind C_{60} -indene or C_{60} -anthracene, whereas encapsulation does not occur in unfunctionalized fullerenes or monoadducts. A cuboctahedron metallacage and the encapsulation of a single-molecule protein are shown in Figure 1e [48], which provides a useful platform for protein-based nanobiotechnology in stabilization and drug delivery.

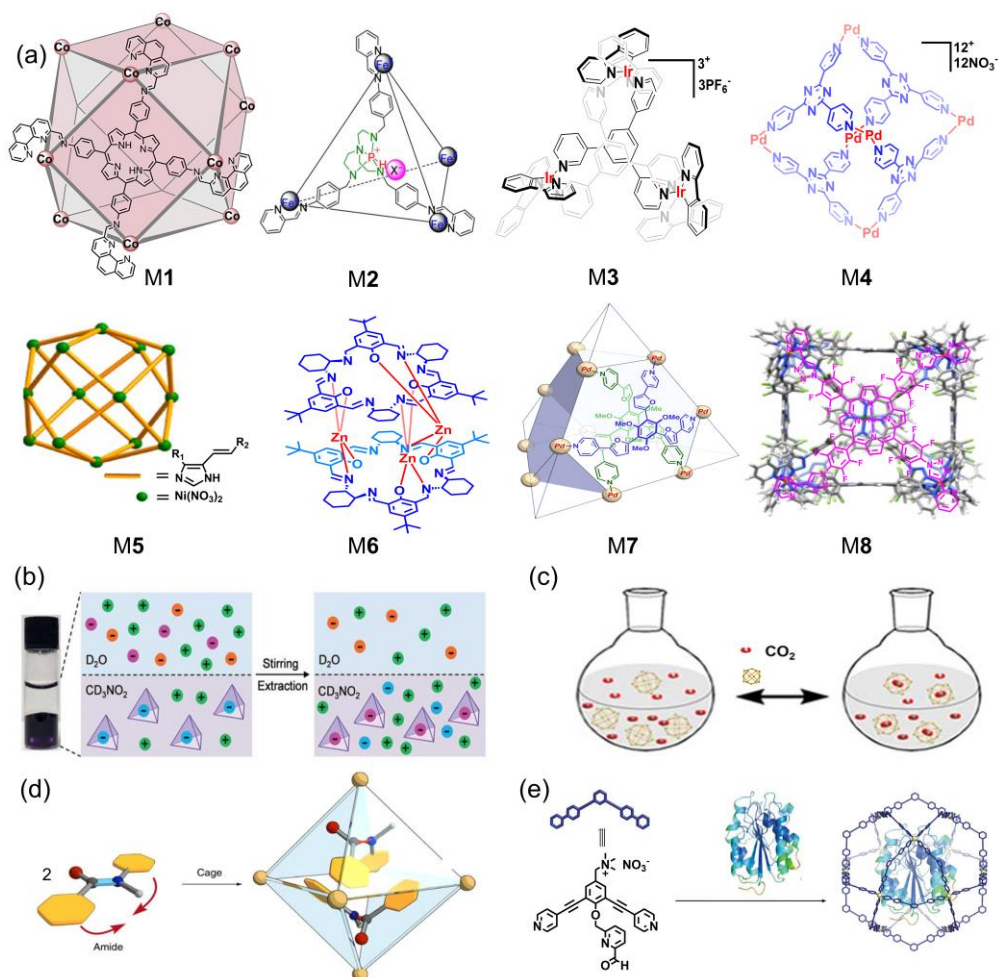


Figure 1. Encapsulation and separation of metallacycles and metallacages. (a) The structures of M1–M8. (b) Selective liquid-liquid extraction of ReO_4^- from water into nitromethane in the existence of other anions. (c) Schematic of the encapsulation of CO_2 by M5 in solution. (d) Schematic of the inclusion of diaryl amide within cage M4. (e) The encapsulation of a single-molecule protein. Adapted with permission from refs. [25,33,37–42,44,49]. Copyright 2017, 2018, 2019 and 2020 American Chemical Society; 2021 Royal Society of Chemistry; 2018 and 2022 Wiley-VCH; 2017, 2020 Nature Publishing Group.

2.2. Catalysis

Due to their designable structure, nanoscale sizes, and adjustable properties, metallacycles and metallacages have excellent potential for application in catalysis and have exhibited catalytic activities for multiple chemical reactions. Hydrogen evolution from the catalysis of metallacages has been studied by different groups. Boomishankar and coworkers used M9 (Figure 2a) as an efficient photocatalyst with the assistance of a photosensitizer and sacrificial electron donor [30], in which the incorporated dye molecules were used to construct a photocatalytic system. By combining with the catalytic sites of Pd²⁺ and two encapsulated fluorescein molecules, heterogenized M10 was designed by Huang and exhibited a high H₂ production rate under visible light [50]. Liu developed a dual-function photocatalyst based on hybrid materials [51], which were composed of metallacages M11 and TiO₂. After loading ReP, the hybrid materials showed selective activity for the photoreduction of CO₂ to CO and produced syngas of CO/H₂ in a CO₂-saturated aqueous solution of dimethylformamide (Figure 2b).

The water oxidation process based on ruthenium catalysis has attracted much attention over the last few years [52,53]. Würthner reported a series of Ru-based trinuclear metallacycles and investigated the impact of substituents [54], sizes [55,56], photosensitizers, and reaction media [57] on the catalytic activity, which deliver excellent supramolecular catalysts for the development of water oxidation. Li prepared a series of Co-based metallacages that could drive water oxidation under visible light [58]. Based on the relationship between the structure and activity, metallacage M12 containing Co-based active sites displayed high catalytic activity and initial oxygen evolution rate. Other catalytic reactions related to metallacycles and metallacages have also been explored. Stang's group constructed two chiral Pt-based metallacycles M13a and M13b and successfully used them for the asymmetric addition reaction of various α,β -enones with styrylboronic acids in high yields (40–98%) and with high enantioselectivities (87–96% ee) [9]. Su constructed an Fe₄L₆ metallacage, M14 [59], which was sufficiently stable under different pH conditions as well as in redox processes. M14 not only acted as a catalyst for the dehydrogenation reaction but also exhibited remarkable continuing and recycling performance. Su prepared metallacage M15 by incorporating the metal complex Ir-6-(4-carboxy-phenyl)-nicotinic acid (Ir-ppyc) into a Zr-based cage [60]. M15 showed a higher selectivity in converting CO₂ reduction under visible light irradiation than the classical metal-organic framework counterpart.

In addition to the above examples, many other metallacycles and metallacages can exhibit excellent catalytic performance regarding different reactions, such as Michael addition reactions [61], the solvolysis of acetal [23], cascade reactions [27], oxygen reduction electrocatalysis [62], and the Strecker reaction [63] among others [62,64,65].

2.3. Biomedical Applications

2.3.1. Drug Encapsulation and Delivery

As host-guest containers, metallacycles and metallacages exhibit fascinating potential in drug delivery applications. Mukherjee and coworkers reported that the hydrophobic cavity of M16 (Figure 3a) with large windows strong candidate for encapsulating and transporting small molecule hydrophobic drugs such as curcumin in an aqueous solution [66]. In addition to enhancing the solubility of curcumin, its inclusion in the cavity prevents it from photodegrading. Mirkin constructed the allosterically regulated metallacage M17 [67]. The asymmetric structure of the receptor was able to transform between a rigid cationic configuration and a flexible neutral configuration using a simple ion, which allowed β -estradiol and dextromethorphan to be selectively bound and reversibly encapsulated into M17. Nanoparticles based on metallacages were also designed for drug encapsulation and delivery. Figure 3b displays the fluorescein-conjugated fluorescein-Pt(IV) prodrug loaded into M4 via host-guest interactions [68]. In addition, Therrien's group has demonstrated the enormous potential of Ru-based metallacages to transport guest molecules such as photosensitizers to cells [69–71]. Research on metallacages as drug carriers was also in-

vestigated, in which other small-molecule drugs, including 5-fluoracil and cisplatin, were transported [72,73].

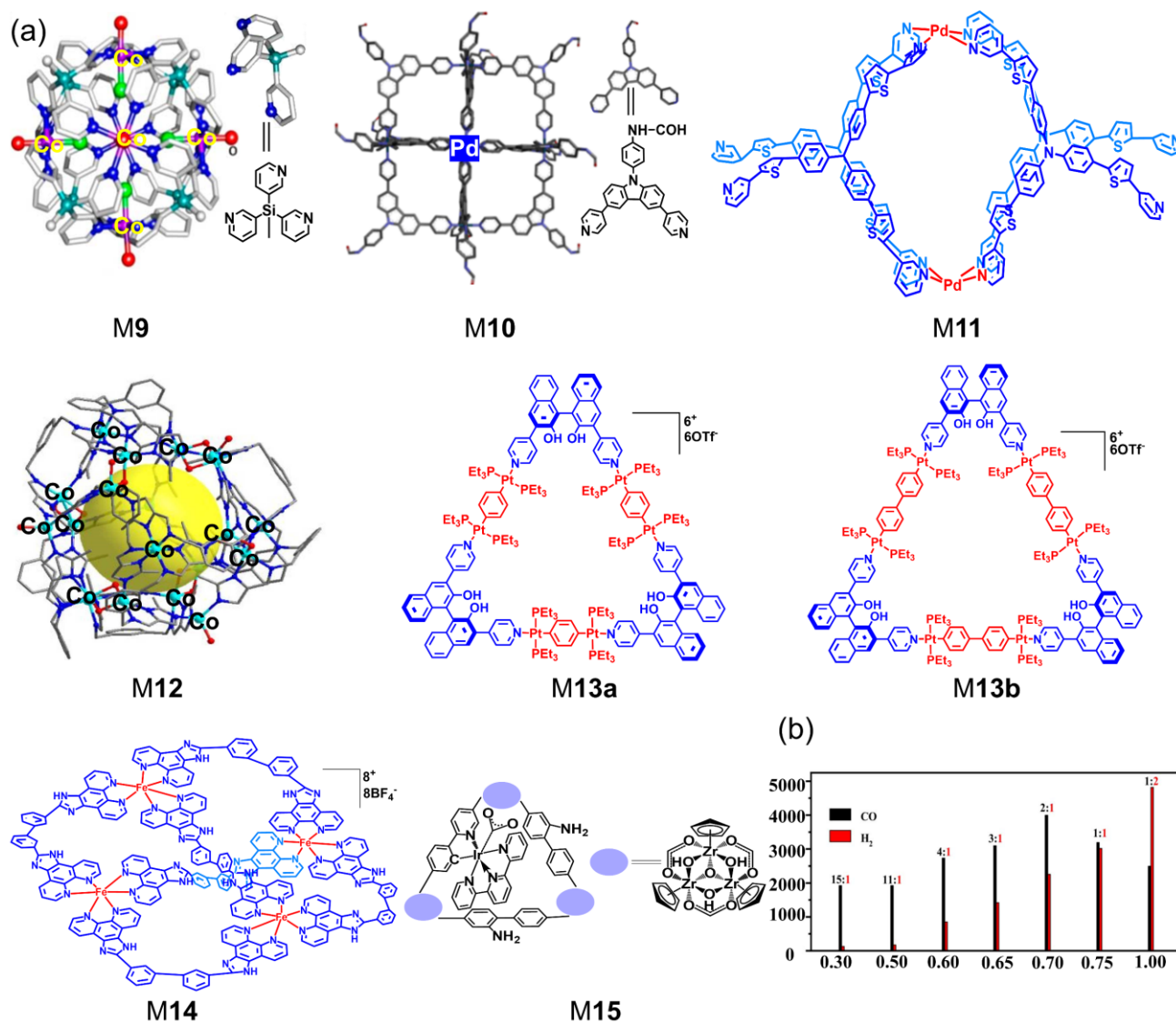


Figure 2. Catalysis of metallacycles and metallages. (a) The structures of M9–M15. (b) Histogram of CO/H₂ generation by ReP/TiO₂-M11 in CO₂-saturated DMF solutions with different water contents for 5 h under visible light. Adapted with permission from refs. [9,30,50,51,58–60]. Copyright 2017, 2020, 2021, and 2022 American Chemical Society.

Metallages that are capable of selectively binding two or more different guests have tremendous advantages in numerous potential applications. In this regard, Crowley designed a Pd₂L₄ multicavity tube-like metallage M18 based on pentapyridyl and hexapyridyl ligands [74]. With multiple discrete binding sites, it was exploited to selectively bind two or more guest molecules (Figure 3c). Nitschke prepared triangular-prismatic Ni(II)-based metallages from two different ligands that were able to bind more than twenty different drugs, natural products, and steroid derivatives within their prolate cavity [75].

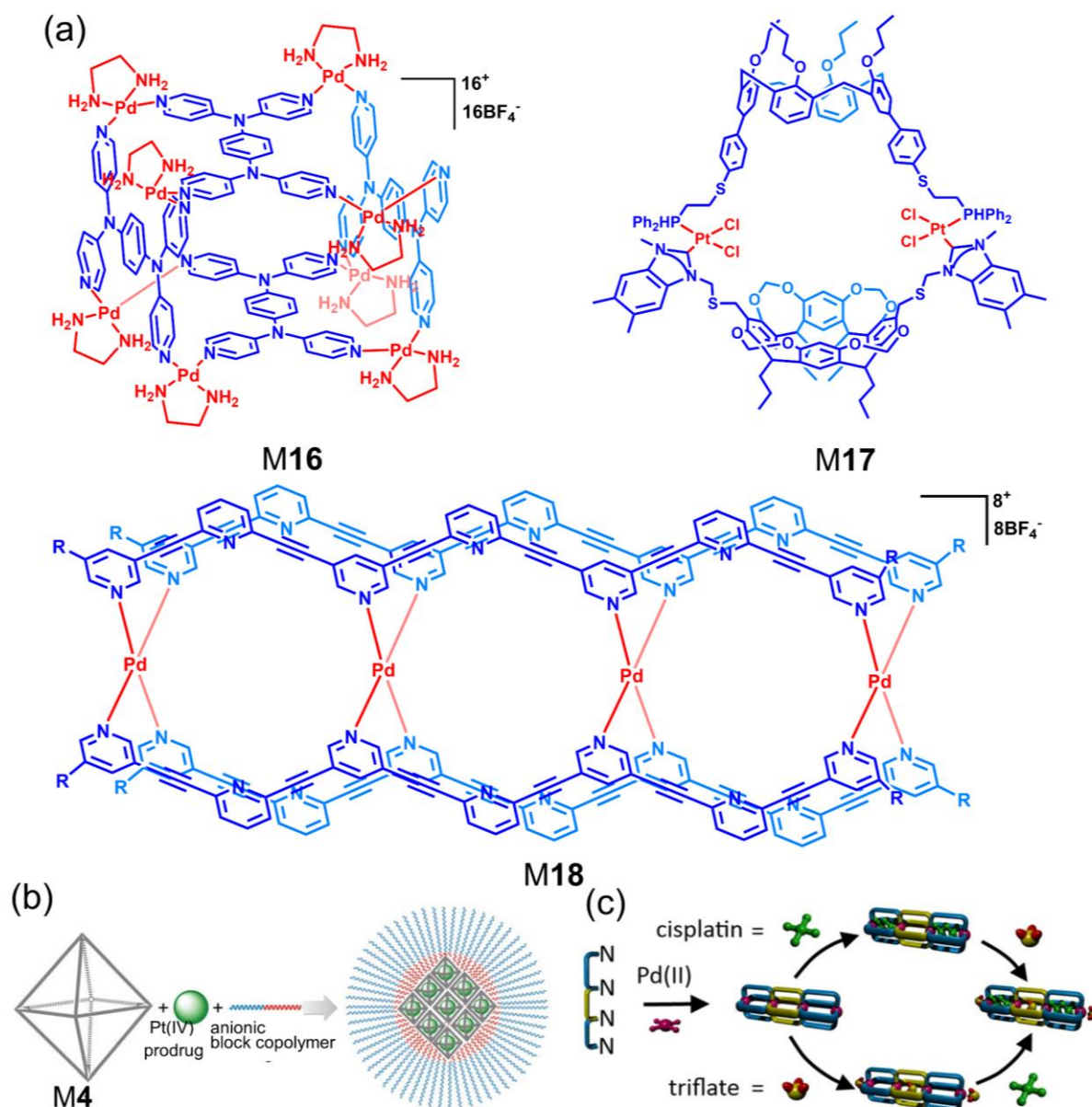


Figure 3. Drug encapsulation and delivery of metallacycles and metallacages. (a) The structures of M16–M18. (b) The nanoformulation of M4 for Pt drug delivery. (c) Selective binding of cisplatin and triflate in cavities. Adapted with permission from refs. [66–68,74]. Copyright 2017 American Chemical Society; 2018 Royal Society of Chemistry.

2.3.2. Biological Recognition and Sensing

The recognition and isolation of metallacycles and metallacages toward complex biomolecules, including amino acids, sucrose, small molecule drugs, etc., make them potential candidates for chemical sensing and biotechnology. Cui et al. synthesized three chiral NH-functionalized fluorescent Zn-based metallacycles, M19a-c (Figure 4a) [31] and demonstrated their high binding affinity and enantioselectivity toward small-molecule pharmaceuticals (L-dopa, D-penicillamine), amino acids, and α -hydroxycarboxylic acids. The strong fluorescence allowed its application in chiral sensing (Figure 4b). Yoshizawa prepared a Pt-based metallacage M20 and reported the efficient and selective encapsulation of D-sucrose from natural disaccharide mixtures in water [76]. Zhang constructed a fluorescent metallacycle-cored supramolecular network by linking metallacycle M21 via a dynamic covalent reaction and showed that it can be used as a chemical sensor to

detect picric acid and halogen ions [77]. Stang and coworkers prepared three multicomponent Pt-based metallacages, M22a-c [78]. Figure 4c demonstrates strong fluorescence sensing and has been utilized as a “turn-on” fluorescent sensor for the detection of thiol-containing amino acids, including cysteine and glutathione, in methanol/water, which follows a self-destructive mechanism. Moreover, M22 can also be regenerated by adding Pt(II) acceptors. Then, they designed a triangular metallosalen-based metallacycle M23, constructed a Pt(II) metallacycle-cored supramolecular network [34], and examined the amino acid sensing capability. The limits of detection for cysteine and glutathione were 79.1 and 15.4 μM , respectively.

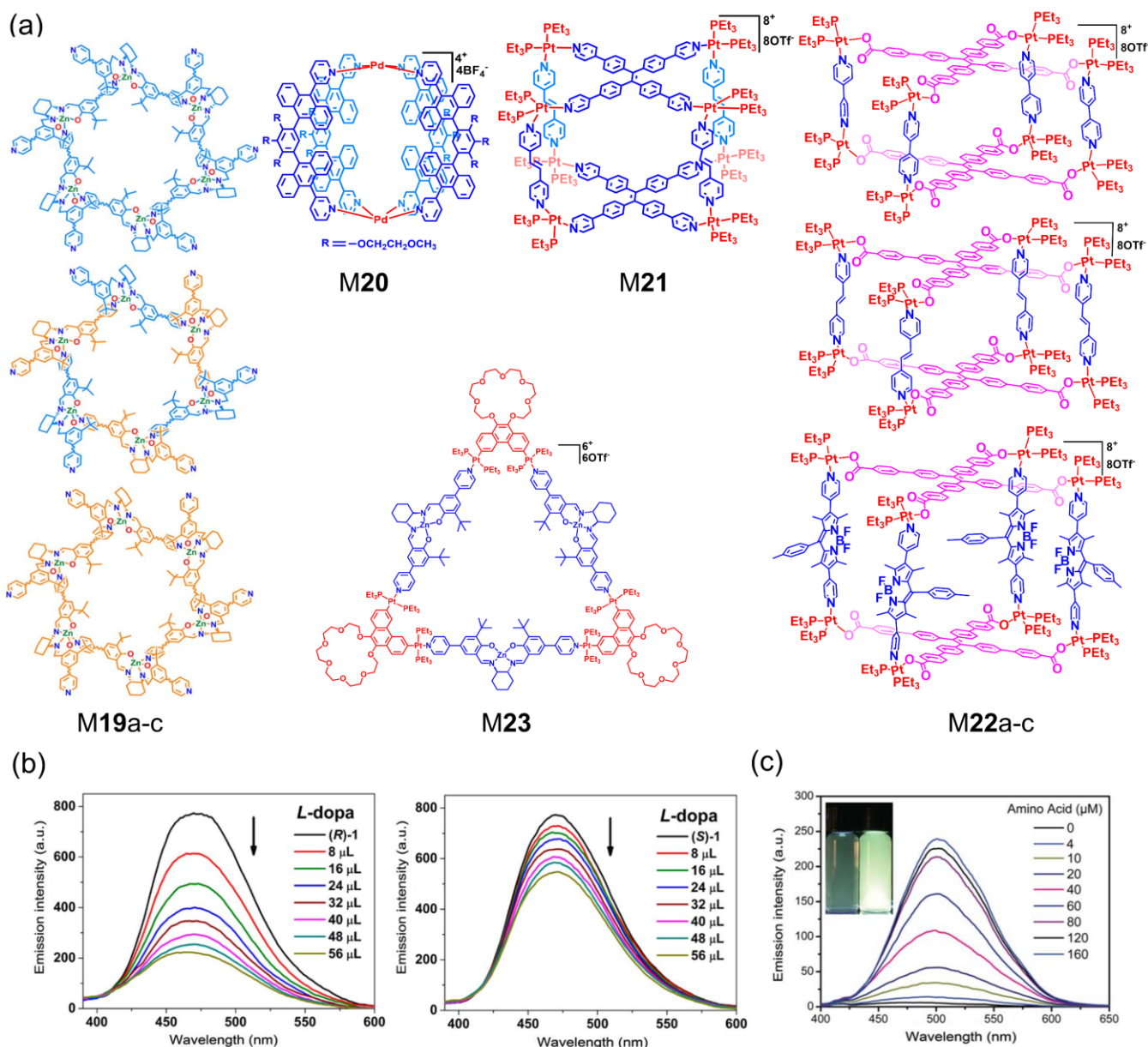


Figure 4. Biological recognition and sensing of metallacycles and metallacages. (a) The structures of M19–M23. (b) Fluorescence emission spectra of (R)- and (S)-M19a (2.0×10^{-6} M in THF) upon titration with L-dopa. (c) Fluorescence spectra of M22 with increasing amounts of thiol-containing amino acids. Adapted with permission from refs. [31,34,76–78]. Copyright 2017 and 2021 American Chemical Society; 2020 Royal Society of Chemistry; 2017 American Association for the Advancement of Science.

2.3.3. DNA Binding

Terenzi engineered three Pt-based quadrangular metallacycles with different sizes and evaluated their affinity for G-quadruplex DNA [79]. The findings showed the interaction between metallacycles and ligands with double-stranded DNA. Sleiman generated a series of square metallacycles of platinum and examined their binding to guanine quadruplexes [80], including oncogene, DNA, and RNA guanine quadruplexes associated with telomeres. This work proved that it is feasible to regulate the binding activity between DNA and metallacycles.

2.3.4. Antibacterial Activity

Some efficient antibacterial systems based on metallacycles and metallacages have been established in recent years [24,81,82]. Li designed and synthesized three nest-like metallacycles and two hexagonal metallacages [83,84], and they all showed remarkable antimicrobial activity. Niu et al. prepared Pt(II)-based metallacycle M24 (Figure 5a) that exhibited aggregation-induced emission (AIE) activity and self-assembled it with tobacco mosaic virus coat protein [85]. The assembly displayed strong membrane-intercalating ability and reactive oxygen species (ROS) generation in bacteria under light irradiation, which resulted in excellent antibacterial activity against gram-positive bacteria. Mukherjee presented a Pd-based metallacage, M25 [86], which exhibited oxidase-like enzymatic behavior even at very low concentrations under white light irradiation. As shown in Figure 5b, exogenous ROS generation has been exploited in efficient photocatalytic and antibacterial activity toward *S. aureus*. Yang's group synthesized a heterometallic triangular necklace-like metallacycle M26 containing Cu(I) and Pt(II) ions [87]. The existence of two metal centers endowed M26 with superior antibacterial activity and nuclease properties, in which bacterium-binding and bacterium-damaging activities against drug-resistant pathogens were shown.

Some metallacycles and metallacages with unique special structures and compositions have antiseptic effects as well as fluorescence imaging. Zhang prepared supramolecular networks by cross-linking hexagonal metallacycle M27 with poly (N-isopropylacrylamide) (PNIPAAm) [88]. M27 exhibits strong fluorescence signals and antibacterial activity for supramolecular networks. Benefiting from the improved bioavailability, supramolecular networks can act as imaging and killing reagents for bacteria. Sun and coworkers designed a hexagonal Pt(II)-based metallacycle M28 [89] and constructed a supramolecular photosensitizer by functionalizing it with pillar [5] arenes through host-guest interactions. The supramolecular photosensitizer showed enhancement in both fluorescence imaging and ROS production capabilities. The results suggested that it can not only track *S. aureus* in situ but also guide the treatment of *S. aureus*-infected mice by fluorescence imaging, and there were no detectable low adverse effects in vitro and in vivo. They also prepared a Ru(II)-based metallacycle M29 with an emissive wavelength beyond ~1000 nm, which showed outstanding optical penetration and excellent antibacterial activity while exhibiting low cytotoxicity to normal mammalian cells [90]. When M29 was prepared in nanoparticles (NPs), accurate bacterial diagnosis and effective phototherapy were performed on *S. aureus*-infected mouse models by NIR-II fluorescence-guided imaging and photoinduced treatments (Figure 5c).

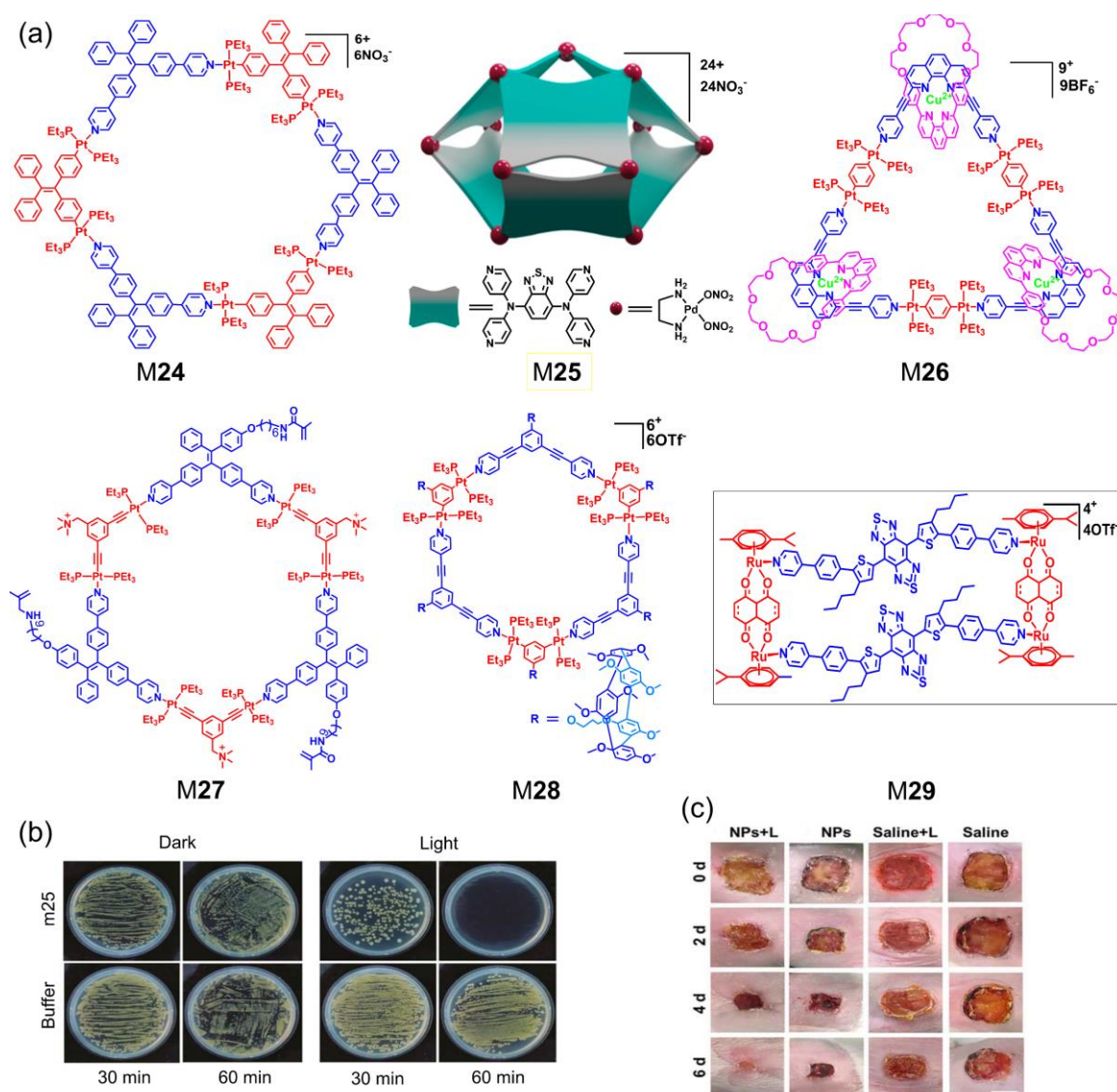


Figure 5. The antibacterial performance of metallacycles and metallacages. (a) The structures of M24–M29. (b) Pictures of the bacterial colonies of *S. bacteria* after exposure to M25 in 0.1 M acetate buffer with white light irradiation. (c) Photographs showing the infected wound after different treatments. Adapted with permission from refs. [85–90]. Copyright 2019 and 2022 National Academy of Sciences (USA); 2020 and 2022 Wiley-VCH; 2020 Nature Publishing Group; 2020 American Chemical Society.

2.3.5. Tumor Imaging and Treatment

Pt-, Pd-, and Ru-based metallacycles and metallacages are widely used in cancer diagnosis and treatment [18,91–94]. Das generated two Pt(II)-based irregular hexagonal metallacycles and studied their cytotoxicity using various cell lines, including the A549, KB, MCF-7, and HaCaT cell lines [95]. The results showed that the smaller metallacycle exhibits better cytotoxic effects. They also prepared two other Pt(II)-based metallacycles with hexagonal shapes and confirmed their anticancer efficiency in comparison to cisplatin [96]. Stang and coworkers produced an effective drug delivery system based on the water-soluble hexagonal metallacycle M30 (Figure 6), which transports curcumin into different cancer cells. The encapsulation of curcumin results in the synergistic enhancement of M30 [97]. Yang presented porphyrin-functionalized star polymers through post-assembly polymerization of a hexagonal Pt(II)-based metallacycle M31 cisplatin [98]. The obtained

metallacycle-linked star polymer showed an excellent ability to enhance cellular uptake and generate $^1\text{O}_2$, and therefore, superior antitumor activity was observed under light irradiation. Combining the fluorescence, anticancer and targeted properties into a single entity, Zhang's group prepared two biotinylated fluorescent Pt(II)-based metallacages, which were successfully employed for bioimaging, cancer treatment, and targeting [99].

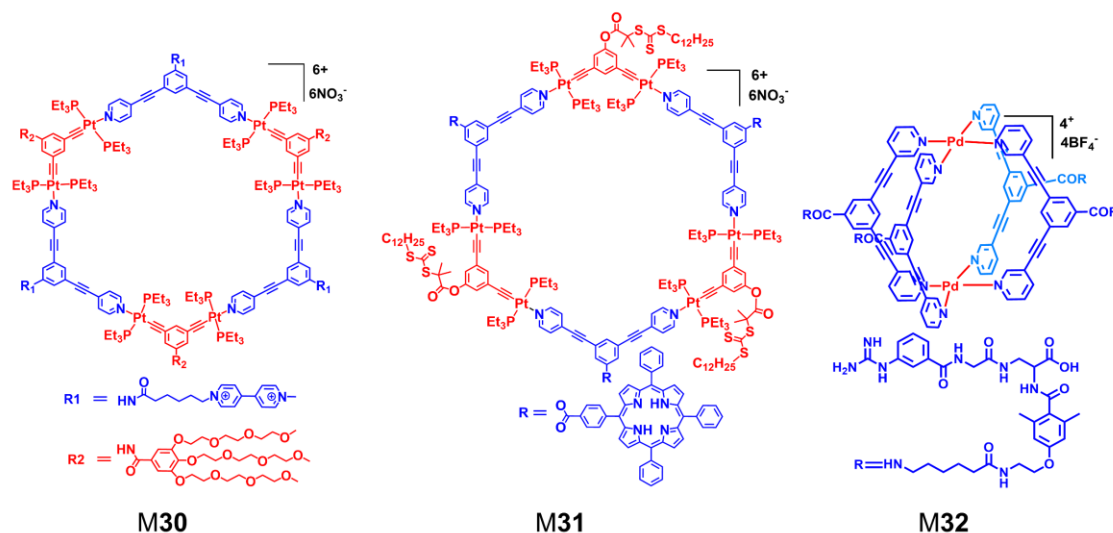


Figure 6. The structures of M30–M32. Adapted with permission from references [18,97,98]. Copyright 2018 National Academy of Sciences (USA); 2018 American Chemical Society; 2019 Royal Society of Chemistry.

The metallacycles and metallacages incorporated anticancer drugs showed better anticancer activity *in vitro* than the precursors, such as cisplatin. Casini et al. designed Pd(II)-based metallacycle M32 and constructed an integrin-selective drug delivery system by conjugating it to different integrin-binding ligands [18]. After encapsulation of cisplatin, the conjugated metallacages exhibited increased anticancer activity *in vitro*, overexpressing $\alpha\text{v}\beta 3$ integrins. Lee prepared four Pd(II)-based metallacycles with triangular or square architectures bearing boron dipyrromethane (BODIPY) ligands [100]. Compared with cisplatin, these metallacycles are highly cytotoxic against U87 glioblastoma cells. In another work, they reported four Pt- or Pd-based octacationic metallacycles from BODIPY ligands [101]. The activities against cell lines showed strong cytotoxicity toward cancer cells compared to cisplatin but exhibited 7.0–15.2 times lower toxicity in normal cells. Mukherjee synthesized four octanuclear Ru(II) metallacages and compared the *in vitro* antitumor effect with that of cisplatin [102]. The very low micromolar IC₅₀ values indicated that their metallacycle that can generate ROS has the greatest anticancer effect against the selected cancer cell lines. Stang synthesized six tetranuclear metallacycles and hexanuclear metallacages by coordination-driven self-assembly and evaluated their cytotoxicity toward human normal and cancer cell lines [103].

To further explore the *in vivo* biological application of metallacycles and metallacages, much research has been carried out. In this respect, Stang and coworkers have published a series of excellent works. They synthesized a four-armed amphiphilic polymer consisting of an AIE metallacycle M33 (Figure 7a) core and GSH-responsive arms [104]. After self-assembly into NPs and vesicles, the small molecule anticancer drugs doxorubicin or doxorubicin hydrochloride were further encapsulated. The results showed that the drug delivery system has a synergistic anticancer effect both *in vitro* and *in vivo*. A suite of Pt(II) drug-loaded metallacycle M34 was designed and synthesized for combination with cancer chemotherapy [105], in which the chemotherapy drugs camptothecin (CPT) and combretastatin A4 (CA4) were loaded in metallacycles. Nanoformulations (NFs) were fabricated by encapsulating M34 into folic acid (FA)-functionalized diblock copolymers,

which exhibited high anticancer efficacy as well as few side effects (Figure 7b). In another study, they prepared NPs by self-assembly of an amphiphilic copolymer, which consisted of H₂O₂-responsive diblock copolymer arms and a hexagonal metallacycle M35 core [106]. The NPs can not only encapsulate doxorubicin and palmitoyl ascorbate but also show excellent antitumor performance with negligible systemic toxicity. The group also prepared a theranostic nanoprobe that incorporated rhomboidal Pt-based metallacycle M36 and NIR-II molecular dye. The applications for cancer diagnosis and treatment are shown in Figure 7c [107]. The nanoprobe provides accurate diagnosis with high resolution and can inhibit tumor growth with fewer adverse reactions than cisplatin via the enhanced permeability and retention (EPR) effect. A dual-emissive Pt-based metallacycle M37 was reported [108]. The NPs formed by M37 and amphiphilic diblock copolymers demonstrate hypoxia imaging as well as chemotherapy in vivo. Mao et al. constructed a theranostic NIR metallacycle M38 and developed it in MNPs for imaging-guided cancer radiochemotherapy, which revealed better antitumor performance against cisplatin-resistant tumors [109]. Zhang synthesized metallacycles M39a-c cored amphiphilic NPs formed by β -CD [110], which not only acted as contrast agents for cell imaging but also displayed increased anticancer activity.

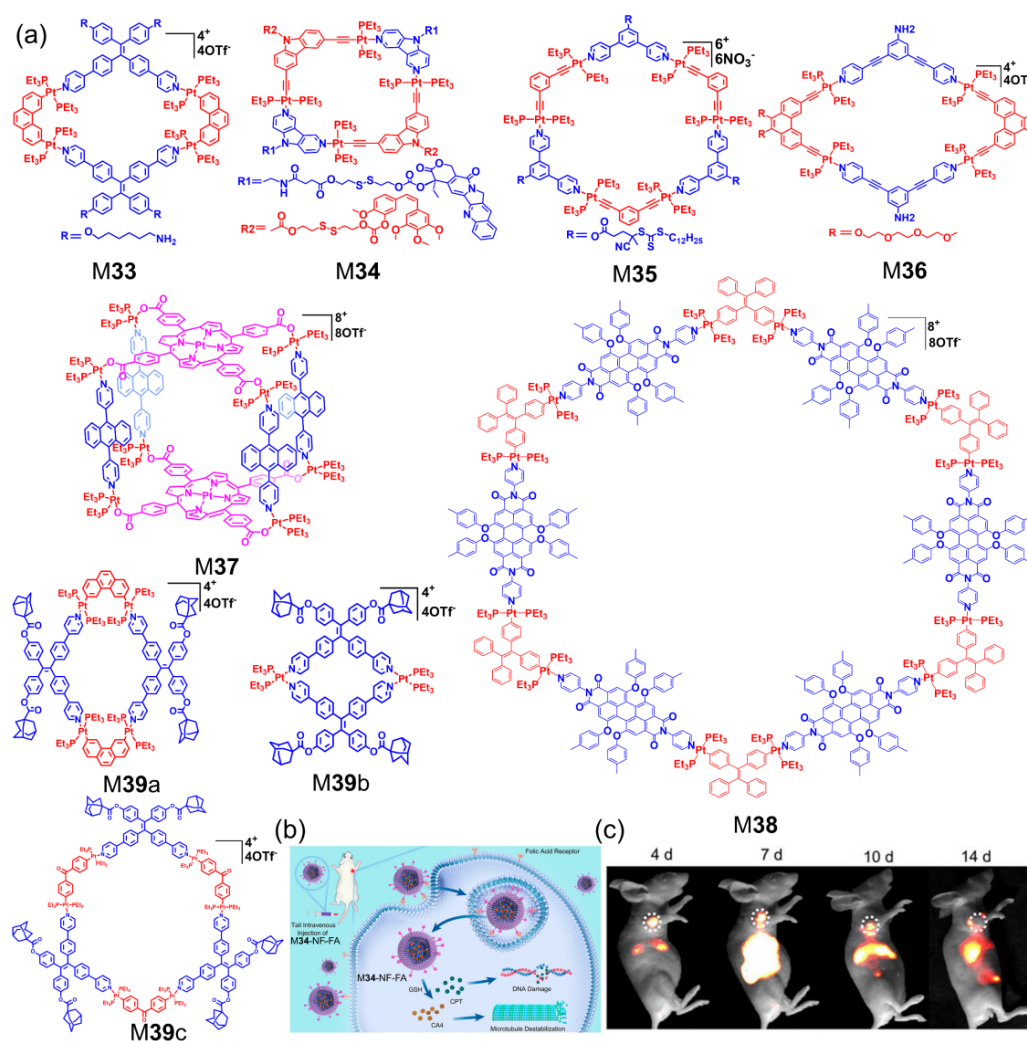


Figure 7. (a) The structures of M33–M39. (b) The cellular uptake of M34-NF-FA and the intracellular release of drugs in response to GSH. (c) NIR-II fluorescence images detecting M36 in tumors. Adapted with permission from refs. [104–110]. Copyright 2017 and 2020 American Chemical Society; 2019 and 2022 National Academy of Sciences (USA); 2020 and 2022 Wiley-VCH.

Due to its excellent therapeutic effects, negligible side effects, and noninvasiveness, photodynamic therapy (PDT) has recently gained increasing attention in cancer treatment. Through the ingenious design of structures, Therrien and coworkers incorporated photosensitizers into Ru-based metallacages and widely investigated their applications in PDT, in which the metallacages showed good therapeutic effects in cancer as well as rheumatoid arthritis [111–113]. Tang synthesized two amphiphilic Pt(II)-based metallacycles, which can potentially be applied to PDT [114]. Stang designed and synthesized Ru-Pt metallacycles and octahedral metallacage M40 (Figure 8a) via a photosensitizer based on Ru(II) and building blocks based on Pt(II), which demonstrated a large two-photon absorption cross-section as well as high efficiency of ROS generation [115]. After encapsulation into a polymer and the formation of NPs, excellent PDT performance was demonstrated in three-dimensional MCs and in vivo studies. They also described two porphyrin-containing Pt(II) metallacages, M41a and M41b, and examined their potential in PDT [116]. In vivo and in vitro investigations indicate the NPs containing M41a and M41b display enhanced antitumor effects with lower dosage requirements and very few adverse effects compared with the precursors. Dong reported an indocyanine green (ICG)-involved photoactive antitumor hexagonal nanoplate based on Pd(II) metallacage M42, which served as an efficient antitumor photosensitizer via PDT for increased NIR light-induced $^1\text{O}_2$ generation, enhanced cellular uptake, and selective targeting ability of lysosomes [117]. Yang designed a dual-stage metallacycle M43 and constructed M43-loaded NPs that realized reversible control of $^1\text{O}_2$ generation [118]. As a promising platform for selective PDT, the dual-stage system exhibits promising anticancer applications.

Some metallacycles and metallacages have been used as therapeutic agents for PTT. Stang et al. reported a rhombic Pt(II)-based metallacycle M44 with high photothermal conversion capacity and encapsulated it into NPs via Pluronic F127, which presented excellent hydrophilicity and biocompatibility [119]. The F127/M44 NPs exhibited enhanced photothermal effects and excellent antitumor PTT behavior in vivo. Zhao and coworkers synthesized a series of Pt(II)-based metallacycles with high photoconversion efficiency for synergistic PDT/PTT therapy [120]. Compared with their precursors, the in vitro studies of M45-NPs showed significant photoconversion, which promoted photoinduced cell injury and subsequently realized tumor ablation.

Multifunctional nanocarrier systems based on metallacycles and metallacages for cancer diagnosis and treatment have undergone great development in recent years. Chen et al. integrated a chemotherapy and PDT strategy utilizing a porphyrin- and Pt(II)-based metallacage M46 (Figure 9a) via multicomponent self-assembly, in which M46 served as a multimodality theranostic platform to fabricate NPs [121]. The cooperation of chemotherapy and PDT exhibited remarkable synergistic antitumor efficacy in vitro and in vivo. Kim constructed an NIR-II nanotherapeutic platform through the incorporation of Pt(II)-based metallacycle M47 and NIR-II dye into F127 [122]. The designed NPs showed high tumor uptake with superior photostability and a high signal-to-noise ratio for real-time guiding therapy, increasing the antitumor efficacy as well as reducing the adverse effects in the U87MG glioblastoma model.

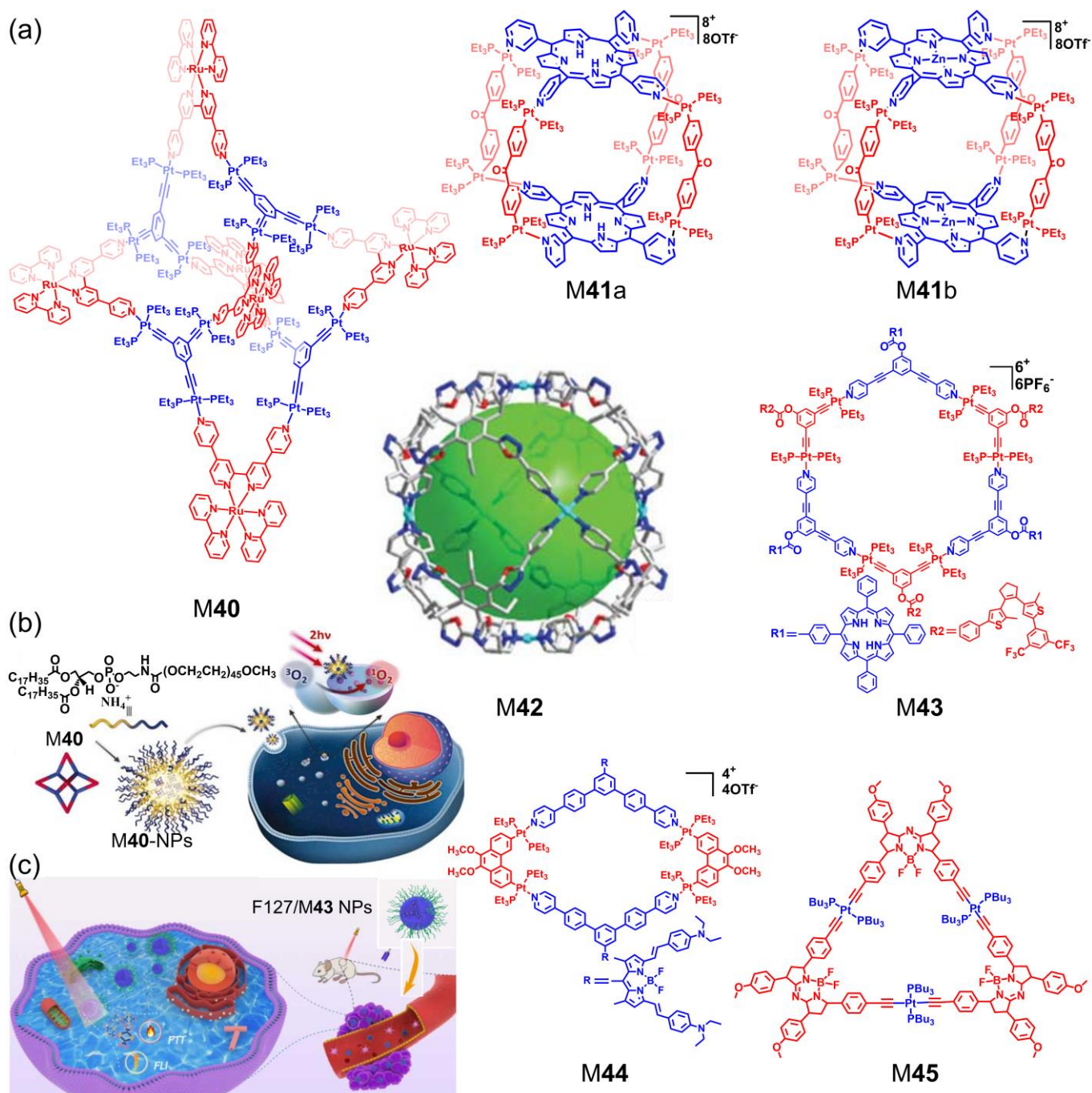


Figure 8. (a) The structures of M40–M45. (b) Schematic illustration of the fabrication, uptake, and accumulation of M40NPs, and their applications in PDT. (c) A schematic illustration of the application of F127/M43 NPs in imaging-guided photothermal therapy. Adapted with permission from refs. [115–120]. Copyright 2019 and 2020 American Chemical Society; 2019 National Academy of Sciences (USA); 2021 Royal Society of Chemistry; 2022 MDPI.

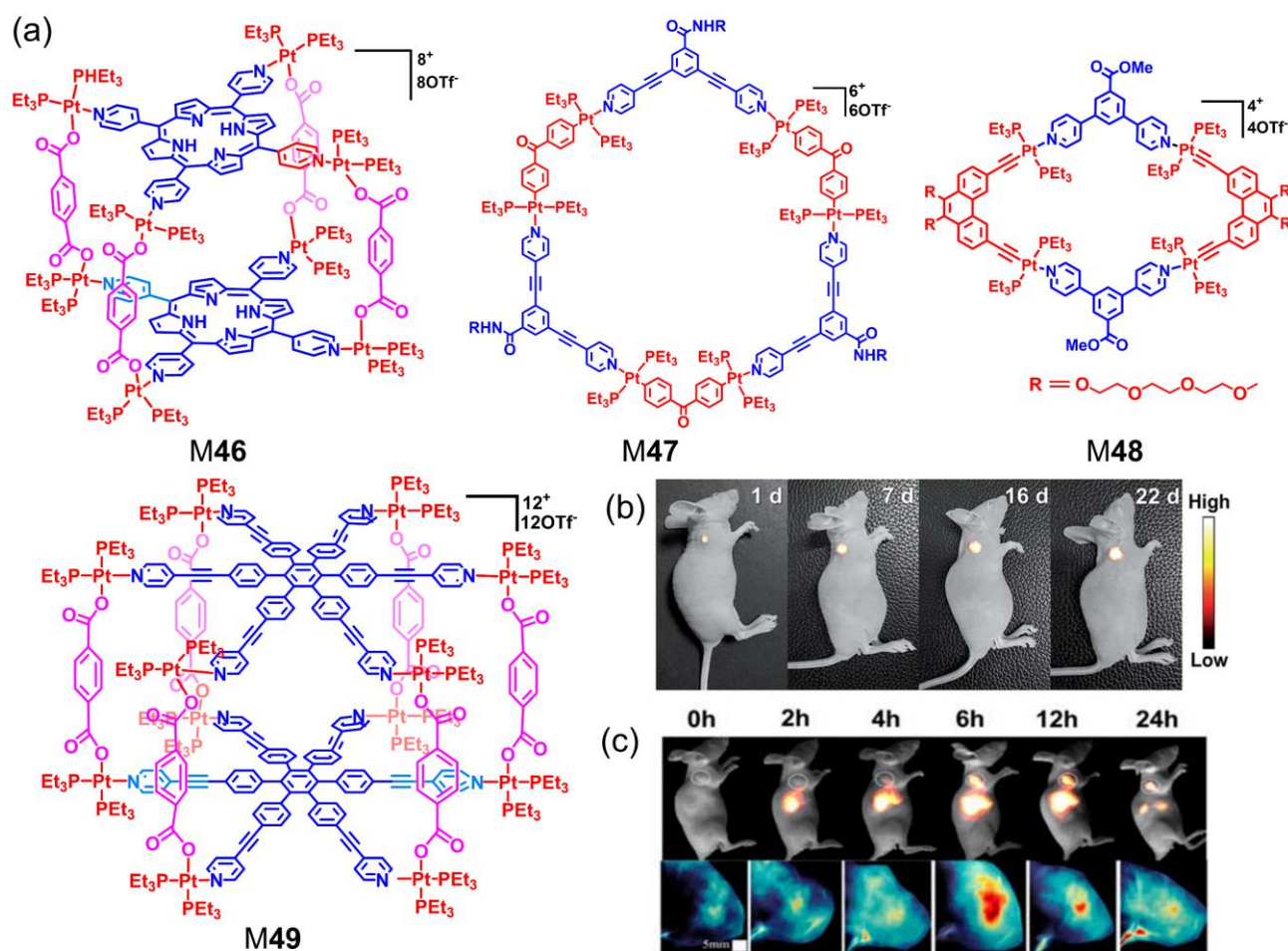


Figure 9. (a) The structures of M46–M49. (b) NIR-II fluorescence images of the M47-based nanoheranostic agent therapeutic response in U87MG tumors. (c) NIR-II fluorescence and PA images of M48-NPs at different times. Adapted with permission from refs. [16,121–123]. Copyright 2019 National Academy of Sciences (USA); 2019 Royal Society of Chemistry; 2018 Nature Publishing Group.

Considering the flexibility and compatibility of photoacoustic (PA) imaging and NIR-II fluorescence imaging, Stang et al. described a dual-modal imaging and chemophotothermal synergistic therapy nanoagent that incorporates metallacycle M48 and NIR-II fluorescent dye into molecular-dye-modified melanin dots [123]. Nanoagents showed both favorable stability and optical properties *in vivo*, as well as passive targeting ability for tumors, and provided a remarkable multifunctional theranostic platform for biomedicine. In addition, they utilized Pt-based metallacycle M49 to encapsulate a photosensitizer and constructed a dual-functionalized system by wrapping it into NPs [16]. The *in vivo* results revealed that synergistic PDT and chemotherapy displayed excellent anticancer behavior toward drug-resistant tumors.

2.4. Other Applications of Metallacycles and Metallacages

Stang's group described Pt(II)-based metallacycles and metallacages that can be used as artificial light-harvesting systems [15,124]. Inspired by the planar chirality of pillararenes, they also prepared metallacycles with chiral optical activities [8]. Metallacycles with high quantum yields and tunable fluorescence wavelengths have been developed in versatile fluorescent materials [125]. A certain quantity of metallacycles and metallacages with specific stimulus-response properties have been made by designing building blocks incorporating functional moieties, such as metal ions [126], temperature [127–130], ligands [131], light [132,133], and enzymes [134].

3. Conclusions and Outlook

Metallacycles and metallacages have attracted widespread attention, not only because of their precise stoichiometry but also due to the flexibility and viability of their design. Specific applications of metallacycles and metallacages have been discussed herein. The diversification in sizes, geometries, and properties, metallacycles, and metallacages have been widely applied in the field of encapsulation, separation, catalysis, biomedicine, and so on. In particular, the employment of metallacycles and metallacages as drug delivery systems, imaging and theranostic platforms have received a lot of attention. Because of their well-defined structures, the cavities of metallacycles and metallacages can encapsulate drugs and transport them to tumor cells, which enhances the bioavailability of hydrophobic drugs and shows good anticancer activity. Through rational design and encapsulation in amphiphilic block copolymers, NPs based on metallacycles and metallacages can also provide a multimodal and synergistic therapeutic platform for precise cancer diagnosis and treatment, including imaging, chemotherapy, PDT, and PTT.

A wide variety of metallacycles and metallacages have been constructed and applied in various fields. However, there are still many challenges. On the one hand, metallacycles and metallacages with more complicated structures and other metal centers in addition to the commonly used Pt and Pd need to be further explored. However, there is an urgent need to translate the existing research into clinical practice, which is an indispensable part of biological applications. To conclude, metallacycles and metallacages are expected to remain attractive and hot topics in materials science.

Author Contributions: Conceptualization and writing, Y.S., P.J.S. and C.Y.; writing—original draft preparation, C.Y.; validation, B.O. and J.D.; writing—review and editing, B.O., Y.S. and P.J.S. All authors have read and agreed to the published version of the manuscript.

Funding: This research was funded by the National Institute of Health grant number R01-CA215157.

Institutional Review Board Statement: Not applicable.

Informed Consent Statement: Not applicable.

Data Availability Statement: Not applicable.

Acknowledgments: Y. Sun thanks the Henan University Third Level Start-up Fund. P.J. Stang is grateful for support by the NIH (grant R01-CA215157).

Conflicts of Interest: The authors declare no conflict of interest.

References

1. Li, B.; He, T.; Fan, Y.; Yuan, X.; Qiu, H.; Yin, S. Recent developments in the construction of metallacycle/metallacage-cored supramolecular polymers via hierarchical self-assembly. *Chem. Commun.* **2019**, *55*, 8036–8059. [[CrossRef](#)] [[PubMed](#)]
2. Hu, Y.-X.; Zhang, X.; Xu, L.; Yang, H.-B. Coordination-Driven Self-assembly of functionalized supramolecular metallacycles: Highlighted research during 2010–2018. *Isr. J. Chem.* **2019**, *59*, 184–196. [[CrossRef](#)]
3. Xu, L.; Wang, Y.-X.; Chen, L.-J.; Yang, H.-B. Construction of multiferrocenyl metallacycles and metallacages via coordination-driven self-assembly: From structure to functions. *Chem. Soc. Rev.* **2015**, *44*, 2148–2167. [[CrossRef](#)] [[PubMed](#)]
4. Li, H.; Yao, Z.-J.; Liu, D.; Jin, G.-X. Multi-component coordination-driven self-assembly toward heterometallic macrocycles and cages. *Coord. Chem. Rev.* **2015**, *293*, 139–157. [[CrossRef](#)]
5. Sun, Y.; Chen, C.; Liu, J.; Stang, P.J. Recent developments in the construction and applications of platinum-based metallacycles and metallacages via coordination. *Chem. Soc. Rev.* **2020**, *49*, 3889–3919. [[CrossRef](#)]
6. Sun, Y.; Tuo, W.; Stang, P.J. Metal-organic cycle-based multistage assemblies. *Proc. Natl. Acad. Sci. USA* **2022**, *119*, e2122398119. [[CrossRef](#)]
7. Sun, Y.; Chen, C.; Stang, P.J. Soft materials with diverse suprastructures via the self-assembly of metal-organic complexes. *Acc. Chem. Res.* **2019**, *52*, 802–817. [[CrossRef](#)]
8. Zhu, H.; Li, Q.; Shi, B.; Xing, H.; Sun, Y.; Lu, S.; Shanguan, L.; Li, X.; Huang, F.; Stang, P.J. Formation of planar chiral platinum triangles via pillar [5]arene for circularly polarized luminescence. *J. Am. Chem. Soc.* **2020**, *142*, 17340–17345. [[CrossRef](#)]
9. Hong, T.; Zhang, Z.; Sun, Y.; Tao, J.-J.; Tang, J.-D.; Xie, C.; Wang, M.; Chen, F.; Xie, S.-S.; Li, S.; et al. Chiral metallacycles as catalysts for asymmetric conjugate addition of styrylboronic acids to α,β -enones. *J. Am. Chem. Soc.* **2020**, *142*, 10244–10249. [[CrossRef](#)]
10. Lin, X.; Chen, F.; Yu, X.; Wang, H.; Qiu, H.; Li, Y.; Yin, S.; Stang, P.J. Phenylthiol-BODIPY-based supramolecular metallacycles for synergistic tumor chemo-photodynamic therapy. *Proc. Natl. Acad. Sci. USA* **2022**, *119*, e2203994119. [[CrossRef](#)]

11. Chang, X.; Zhou, Z.; Shang, C.; Wang, G.; Wang, Z.; Qi, Y.; Li, Z.-Y.; Wang, H.; Cao, L.; Li, X. Coordination-driven self-assembled metallacycles incorporating pyrene: Fluorescence mutability, tunability, and aromatic amine sensing. *J. Am. Chem. Soc.* **2019**, *141*, 1757–1765. [[CrossRef](#)]
12. Acharyya, K.; Bhattacharyya, S.; Lu, S.; Sun, Y.; Mukherjee, P.S.; Stang, P.J. Emissive platinum(II) macrocycles as tunable cascade energy transfer scaffolds. *Angew. Chem. Int. Ed.* **2022**, *61*, e202200715. [[CrossRef](#)] [[PubMed](#)]
13. Datta, S.; Saha, M.L.; Stang, P.J. Hierarchical assemblies of supramolecular coordination complexes. *Acc. Chem. Res.* **2018**, *51*, 2047–2063. [[CrossRef](#)]
14. Fink, D.; Orth, N.; Linseis, M.; Ivanović-Burmazović, I.; Winter, R.F. Ring size matters: Supramolecular isomerism in self-assembled redox-active tetra- and hexaruthenium macrocycles. *Chem. Commun.* **2020**, *56*, 1062–1065. [[CrossRef](#)] [[PubMed](#)]
15. Li, Y.; Rajasree, S.S.; Lee, G.Y.; Yu, J.; Tang, J.-H.; Ni, R.; Li, G.; Houk, K.N.; Deria, P.; Stang, P.J. Anthracene-triphenylamine-based platinum(II) metallacages as synthetic light-harvesting assembly. *J. Am. Chem. Soc.* **2021**, *143*, 2908–2919. [[CrossRef](#)] [[PubMed](#)]
16. Yu, G.; Zhu, B.; Shao, L.; Zhou, J.; Saha, M.L.; Shi, B.; Zhang, Z.; Hong, T.; Li, S.; Chen, X.; et al. Host-guest complexation-mediated codelivery of anticancer drug and photosensitizer for cancer photochemotherapy. *Proc. Natl. Acad. Sci. USA* **2019**, *116*, 6618–6623. [[CrossRef](#)]
17. Ye, Y.; Cook, T.R.; Wang, S.-P.; Wu, J.; Li, S.; Stang, P.J. Self-assembly of chiral metallacycles and metallacages from a directionally adaptable BINOL-derived donor. *J. Am. Chem. Soc.* **2015**, *137*, 11896–11899. [[CrossRef](#)]
18. Han, J.; Räder, A.F.B.; Reichart, F.; Aikman, B.; Wenzel, M.N.; Woods, B.; Weinmüller, M.; Ludwig, B.S.; Stürup, S.; Groothuis, G.M.M.; et al. Bioconjugation of supramolecular metallacages to integrin ligands for targeted delivery of cisplatin. *Bioconjugate Chem.* **2018**, *29*, 3856–3865. [[CrossRef](#)]
19. Sun, Y.; Yao, Y.; Wang, H.; Fu, W.X.; Chen, C.Y.; Saha, M.L.; Zhang, M.M.; Datta, S.; Zhou, Z.X.; Yu, H.X.; et al. Self-assembly of metallacages into multidimensional suprastructures with tunable emissions. *J. Am. Chem. Soc.* **2018**, *140*, 12819–12828. [[CrossRef](#)]
20. Oldacre, A.N.; Friedman, A.E.; Cook, T.R. A self-assembled cofacial cobalt porphyrin prism for oxygen reduction catalysis. *J. Am. Chem. Soc.* **2017**, *139*, 1424–1427. [[CrossRef](#)]
21. Paul, L.E.H.; Therrien, B.; Furrer, J. Interactions of arene ruthenium metallaprisms with human proteins. *Org. Biomol. Chem.* **2015**, *13*, 946–953. [[CrossRef](#)] [[PubMed](#)]
22. Fink, D.; Orth, N.; Ebel, V.; Gogesch, F.S.; Staiger, A.; Linseis, M.; Ivanović-Burmazović, I.; Winter, R.F. Self-assembled redox-active tetraruthenium macrocycles with large intracyclic cavities. *Organometallics* **2020**, *39*, 1861–1880. [[CrossRef](#)]
23. Holloway, L.R.; Bogie, P.M.; Lyon, Y.; Ngai, C.; Miller, T.F.; Julian, R.R.; Hooley, R.J. Tandem reactivity of a self-assembled cage catalyst with endohedral acid groups. *J. Am. Chem. Soc.* **2018**, *140*, 8078–8081. [[CrossRef](#)] [[PubMed](#)]
24. Malina, J.; Scott, P.; Brabec, V. Recognition of DNA/RNA bulges by antimicrobial and antitumor metallohelices. *Dalton Trans.* **2015**, *44*, 14656–14665. [[CrossRef](#)]
25. Sunohara, H.; Koyamada, K.; Takezawa, H.; Fujita, M. An Ir₃L₂ complex with anion binding pockets: Photocatalytic E-Z isomerization via molecular recognition. *Chem. Commun.* **2021**, *57*, 9300–9302. [[CrossRef](#)]
26. Gupta, G.; Denoyelle-Di-Muro, E.; Mbakidi, J.-P.; Leroy-Lhez, S.; Sol, V.; Therrien, B. Delivery of porphyrin to cancer cells by organometallic Rh(III) and Ir(III) metallacages. *J. Organomet. Chem.* **2015**, *787*, 44–50. [[CrossRef](#)]
27. Jiao, J.; Li, Z.; Qiao, Z.; Li, X.; Liu, Y.; Dong, J.; Jiang, J.; Cui, Y. Design and self-assembly of hexahedral coordination cages for cascade reactions. *Nat. Commun.* **2018**, *9*, 4423. [[CrossRef](#)]
28. Wang, S.; Gao, X.; Hang, X.; Zhu, X.; Han, H.; Liao, W.; Chen, W. Ultrafine Pt nanoclusters confined in a calixarene-Based {Ni₂₄} coordination cage for high-efficient hydrogen evolution reaction. *J. Am. Chem. Soc.* **2016**, *138*, 16236–16239. [[CrossRef](#)]
29. Jing, X.; He, C.; Yang, Y.; Duan, C. A metal-organic tetrahedron as a redox vehicle to encapsulate organic dyes for photocatalytic proton reduction. *J. Am. Chem. Soc.* **2015**, *137*, 3967–3974. [[CrossRef](#)]
30. Deshmukh, M.S.; Mane, V.S.; Kumbhar, A.S.; Boomishankar, R. Light-driven hydrogen evolution from water by a tripodal silane based Co^{II}₆L₁₈ octahedral cage. *Inorg. Chem.* **2017**, *56*, 13286–13292. [[CrossRef](#)]
31. Dong, J.; Tan, C.; Zhang, K.; Liu, Y.; Low, P.J.; Jiang, J.; Cui, Y. Chiral NH-controlled supramolecular metallacycles. *J. Am. Chem. Soc.* **2017**, *139*, 1554–1564. [[CrossRef](#)] [[PubMed](#)]
32. Tang, J.-H.; Li, Y.; Wu, Q.; Wang, Z.; Hou, S.; Tang, K.; Sun, Y.; Wang, H.; Wang, H.; Lu, C.; et al. Single-molecule level control of host-guest interactions in metallocycle-C₆₀ complexes. *Nat. Commun.* **2019**, *10*, 4599. [[CrossRef](#)] [[PubMed](#)]
33. Xie, S.-M.; Fu, N.; Li, L.; Yuan, B.-Y.; Zhang, J.-H.; Li, Y.-X.; Yuan, L.-M. Homochiral metal-organic cage for gas chromatographic separations. *Anal. Chem.* **2018**, *90*, 9182–9188. [[CrossRef](#)] [[PubMed](#)]
34. Zhang, Q.; Chen, F.; Shen, X.; He, T.; Qiu, H.; Yin, S.; Stang, P.J. Self-healing metallacycle-cored supramolecular polymers based on a metal-salen complex constructed by orthogonal metal coordination and host-guest interaction with amino acid sensing. *ACS Macro Lett.* **2021**, *10*, 873–879. [[CrossRef](#)]
35. Yin, C.; Xiao, P.; Liang, M.; Li, J.; Sun, Y.; Jiang, X.; Wu, W. Effects of iRGD conjugation density on the in vitro and in vivo properties of cylindrical polymer brushes. *Biomater. Sci.* **2022**, *10*, 3236–3244. [[CrossRef](#)]
36. Yin, C.; Wang, R.; Sun, Y.; Li, S.; Zhang, X.; Gu, J.; Wu, W.; Jiang, X. The in vitro and in vivo properties of ringlike polymer brushes. *Nano Today* **2021**, *41*, 101293. [[CrossRef](#)]
37. Rizzuto, F.J.; Nitschke, J.R. Stereochemical plasticity modulates cooperative binding in a Co^{II}₁₂L₆ cuboctahedron. *Nat. Chem.* **2017**, *9*, 903–908. [[CrossRef](#)]

38. Zhang, D.; Ronson, T.K.; Mosquera, J.; Martinez, A.; Guy, L.; Nitschke, J.R. Anion binding in water drives structural adaptation in an azaphosphatrane-functionalized $\text{Fe}^{\text{II}}_4\text{L}_4$ tetrahedron. *J. Am. Chem. Soc.* **2017**, *139*, 6574–6577. [[CrossRef](#)]
39. Zhang, D.; Ronson, T.K.; Mosquera, J.; Martinez, A.; Nitschke, J.R. Selective anion extraction and recovery using a $\text{Fe}^{\text{II}}_4\text{L}_4$ cage. *Angew. Chem. Int. Ed.* **2018**, *57*, 3717–3721. [[CrossRef](#)]
40. Tabuchi, R.; Takezawa, H.; Fujita, M. Selective confinement of rare-earth-metal hydrates by a capped metallo-cage under aqueous conditions. *Angew. Chem. Int. Ed.* **2022**, *134*, e202208866. [[CrossRef](#)]
41. Zhang, X.; Dong, X.; Lu, W.; Luo, D.; Zhu, X.W.; Li, X.; Zhou, X.P.; Li, D. Fine-tuning apertures of metal-organic cages: Encapsulation of carbon dioxide in solution and solid state. *J. Am. Chem. Soc.* **2019**, *141*, 11621–11627. [[CrossRef](#)] [[PubMed](#)]
42. Takezawa, H.; Shitozawa, K.; Fujita, M. Enhanced reactivity of twisted amides inside a molecular cage. *Nat. Chem.* **2020**, *12*, 574–578. [[CrossRef](#)] [[PubMed](#)]
43. Takezawa, H.; Fujii, Y.; Murase, T.; Fujita, M. Electrophilic spirocyclization of a 2-biphenylacetylene via conformational fixing within a hollow-cage host. *Angew. Chem. Int. Ed.* **2022**, *134*, e202203970. [[CrossRef](#)]
44. Tamura, Y.; Takezawa, H.; Fujita, M. A double-walled knotted cage for guest-adaptive molecular recognition. *J. Am. Chem. Soc.* **2020**, *142*, 5504–5508. [[CrossRef](#)]
45. Zhang, M.; Xu, H.; Wang, M.; Saha, M.L.; Zhou, Z.; Yan, X.; Wang, H.; Li, X.; Huang, F.; She, N.; et al. Platinum(II)-based convex trigonal-prismatic cages via coordination-driven self-assembly and C_{60} encapsulation. *Inorg. Chem.* **2017**, *56*, 12498–12504. [[CrossRef](#)] [[PubMed](#)]
46. Chang, X.; Lin, S.; Wang, G.; Shang, C.; Wang, Z.; Liu, K.; Fang, Y.; Stang, P.J. Self-assembled perylene bisimide-cored trigonal prism as an electron-deficient host for C_{60} and C_{70} driven by “like dissolves like”. *J. Am. Chem. Soc.* **2020**, *142*, 15950–15960. [[CrossRef](#)]
47. Struch, N.; Bannwarth, C.; Ronson, T.K.; Lorenz, Y.; Mienert, B.; Wagner, N.; Engeser, M.; Bill, E.; Puttreddy, R.; Rissanen, K.; et al. An octanuclear metallosupramolecular cage designed to exhibit spin-crossover behavior. *Angew. Chem. Int. Ed.* **2017**, *56*, 4930–4935. [[CrossRef](#)]
48. Fujita, D.; Suzuki, R.; Fujii, Y.; Yamada, M.; Nakama, T.; Matsugami, A.; Hayashi, F.; Weng, J.-K.; Yagi-Utsumi, M.; Fujita, M. Protein stabilization and refolding in a gigantic self-assembled cage. *Chem* **2021**, *7*, 2672–2683. [[CrossRef](#)]
49. Brenner, W.; Ronson, T.K.; Nitschke, J.R. Separation and selective formation of fullerene adducts within an $\text{M}^{\text{II}}_8\text{L}_6$ cage. *J. Am. Chem. Soc.* **2017**, *139*, 75–78. [[CrossRef](#)]
50. Hou, C.P.; Chen, X.L.; Huang, Z.J.; Lei, Y.; Xiao, L.M.; Huang, J.F.; Li, S.Y.; Liu, J.M. Robust heterogeneous photocatalyst for visible-light-driven hydrogen evolution promotion: Immobilization of a fluorescein dye-encapsulated metal-organic cage on TiO_2 . *ACS Appl. Mater. Interfaces* **2021**, *13*, 57230–57240. [[CrossRef](#)]
51. Qin, S.; Lei, Y.; Huang, J.-F.; Lv, C.-Y.; Li, X.-A.; Su, P.-Y.; Liu, J.-M. Controllable visible-light-driven syngas evolution by a ternary titania hybrid sacrificial system with a photosensitive metal-organic Pd^{II} cage and Re^{I} catalyst. *ACS Sustain. Chem. Eng.* **2022**, *10*, 8254–8264. [[CrossRef](#)]
52. Kunz, V.; Schulze, M.; Schmidt, D.; Würthner, F. Trinuclear ruthenium macrocycles: Toward supramolecular water oxidation catalysis in pure water. *ACS Energy Lett.* **2017**, *2*, 288–293. [[CrossRef](#)]
53. Schulze, M.; Kunz, V.; Frischmann, P.D.; Würthner, F. A supramolecular ruthenium macrocycle with high catalytic activity for water oxidation that mechanistically mimics photosystem II. *Nat. Chem.* **2016**, *8*, 576–583. [[CrossRef](#)] [[PubMed](#)]
54. Meza-Chincha, A.-L.; Lindner, J.O.; Schindler, D.; Schmidt, D.; Krause, A.-M.; Röhr, M.I.S.; Mitrić, R.; Würthner, F. Impact of substituents on molecular properties and catalytic activities of trinuclear Ru macrocycles in water oxidation. *Chem. Sci.* **2020**, *11*, 7654–7664. [[CrossRef](#)] [[PubMed](#)]
55. Kunz, V.; Lindner, J.O.; Schulze, M.; Röhr, M.I.S.; Schmidt, D.; Mitrić, R.; Würthner, F. Cooperative water oxidation catalysis in a series of trinuclear metallosupramolecular ruthenium macrocycles. *Energy Environ. Sci.* **2017**, *10*, 2137–2153. [[CrossRef](#)]
56. Schindler, D.; Meza-Chincha, A.-L.; Roth, M.; Würthner, F. Structure-activity relationship for di-up to tetranuclear macrocyclic ruthenium catalysts in homogeneous water oxidation. *Chem. Eur. J.* **2021**, *27*, 16938–16946. [[CrossRef](#)]
57. Meza-Chincha, A.-L.; Schindler, D.; Natali, M.; Würthner, F. Effects of photosensitizers and reaction media on light-driven water oxidation with trinuclear ruthenium macrocycles. *ChemPhotoChem* **2021**, *5*, 173–183. [[CrossRef](#)]
58. Chen, Z.Y.; Long, Z.H.; Wang, X.Z.; Zhou, J.Y.; Wang, X.S.; Zhou, X.P.; Li, D. Cobalt-based metal-organic cages for visible-light-driven water oxidation. *Inorg. Chem.* **2021**, *60*, 10380–10386. [[CrossRef](#)]
59. Lu, Y.L.; Song, J.Q.; Qin, Y.H.; Guo, J.; Huang, Y.H.; Zhang, X.D.; Pan, M.; Su, C.Y. A redox-active supramolecular Fe_4L_6 cage based on organic vertices with acid-base-dependent charge tunability for dehydrogenation catalysis. *J. Am. Chem. Soc.* **2022**, *144*, 8778–8788. [[CrossRef](#)]
60. Qi, X.; Zhong, R.; Chen, M.; Sun, C.; You, S.; Gu, J.; Shan, G.; Cui, D.; Wang, X.; Su, Z. Single metal-organic cage decorated with an Ir(III) complex for CO_2 photoreduction. *ACS Catal.* **2021**, *11*, 7241–7248. [[CrossRef](#)]
61. Bhat, I.A.; Devaraj, A.; Howlader, P.; Chi, K.-W.; Mukherjee, P.S. Preparation of a chiral Pt_{12} tetrahedral cage and its use in catalytic Michael addition reaction. *Chem. Commun.* **2018**, *54*, 4814–4817. [[CrossRef](#)] [[PubMed](#)]
62. Oldacre, A.N.; Crawley, M.R.; Friedman, A.E.; Cook, T.R. Tuning the activity of heterogeneous cofacial cobalt porphyrins for oxygen reduction electrocatalysis through self-assembly. *Chem. Eur. J.* **2018**, *24*, 10984–10987. [[CrossRef](#)] [[PubMed](#)]

63. Liang, G.M.; Xiong, P.; Azam, K.; Ni, Q.L.; Zeng, J.Q.; Gui, L.C.; Wang, X.J. A discrete tetrahedral indium cage as an efficient heterogeneous catalyst for the fixation of CO₂ and the strecker reaction of ketones. *Inorg. Chem.* **2020**, *59*, 1653–1659. [[CrossRef](#)] [[PubMed](#)]
64. Hong, C.M.; Bergman, R.G.; Raymond, K.N.; Toste, F.D. Self-assembled tetrahedral hosts as supramolecular catalysts. *Acc. Chem. Res.* **2018**, *51*, 2447–2455. [[CrossRef](#)]
65. Jing, X.; He, C.; Zhao, L.; Duan, C. Photochemical properties of host-guest supramolecular systems with structurally confined metal-organic capsules. *Int. J. Antimicrob. Agents* **2019**, *52*, 100–109. [[CrossRef](#)] [[PubMed](#)]
66. Bhat, I.A.; Jain, R.; Siddiqui, M.M.; Saini, D.K.; Mukherjee, P.S. Water-soluble Pd₈L₄ self-assembled molecular barrel as an aqueous carrier for hydrophobic curcumin. *Inorg. Chem.* **2017**, *56*, 5352–5360. [[CrossRef](#)]
67. Mendez-Arroyo, J.; d’Aquino, A.I.; Chinen, A.B.; Manraj, Y.D.; Mirkin, C.A. Reversible and selective encapsulation of dextromethorphan and beta-estradiol using an asymmetric molecular capsule assembled via the weak-link approach. *J. Am. Chem. Soc.* **2017**, *139*, 1368–1371. [[CrossRef](#)]
68. Yue, Z.; Wang, H.; Bowers, D.J.; Gao, M.; Stilgenbauer, M.; Nielsen, F.; Shelley, J.T.; Zheng, Y.-R. Nanoparticles of metal-organic cages designed to encapsulate platinum-based anticancer agents. *Dalton Trans.* **2018**, *47*, 670–674. [[CrossRef](#)]
69. Garci, A.; Mbakidi, J.-P.; Chaleix, V.; Sol, V.; Orhan, E.; Therrien, B. Tunable arene ruthenium metallaprisms to transport, shield, and release porphyrin in cancer cells. *Organometallics* **2015**, *34*, 4138–4146. [[CrossRef](#)]
70. Mannancheril, V.; Therrien, B. Strategies toward the enhanced permeability and retention effect by increasing the molecular weight of arene ruthenium metallaassemblies. *Inorg. Chem.* **2018**, *57*, 3626–3633. [[CrossRef](#)]
71. Gallardo-Villagrán, M.; Paulus, L.; Charissoux, J.-L.; Sutour, S.; Vergne-Salle, P.; Leger, D.Y.; Liagre, B.; Therrien, B. Evaluation of ruthenium-based assemblies as carriers of photosensitizers to treat rheumatoid arthritis by photodynamic therapy. *Pharmaceutics* **2021**, *13*, 2104. [[CrossRef](#)] [[PubMed](#)]
72. Xu, W.-Q.; Fan, Y.-Z.; Wang, H.-P.; Teng, J.; Li, Y.-H.; Chen, C.-X.; Fenske, D.; Jiang, J.-J.; Su, C.-Y. Investigation of binding behavior between drug molecule 5-fluoracil and M₄L₄-type tetrahedral cages: Selectivity, capture, and release. *Chem. Eur. J.* **2017**, *23*, 3542–3547. [[CrossRef](#)] [[PubMed](#)]
73. Woods, B.; Wenzel, M.N.; Williams, T.; Thomas, S.R.; Jenkins, R.L.; Casini, A. Exo-functionalized metallacages as host-guest systems for the anticancer drug cisplatin. *Front. Chem.* **2019**, *7*, 68. [[CrossRef](#)] [[PubMed](#)]
74. Preston, D.; Lewis, J.E.M.; Crowley, J.D. Multicavity [Pd_nL₄]²ⁿ⁺ cages with controlled segregated binding of different guests. *J. Am. Chem. Soc.* **2017**, *139*, 2379–2386. [[CrossRef](#)]
75. Rizzuto, F.J.; Carpenter, J.P.; Nitschke, J.R. Multisite binding of drugs and natural products in an entropically favorable, heteroleptic receptor. *J. Am. Chem. Soc.* **2019**, *141*, 9087–9095. [[CrossRef](#)] [[PubMed](#)]
76. Yamashina, M.; Akita, M.; Hasegawa, T.; Hayashi, S.; Yoshizawa, M. A polyaromatic nanocapsule as a sucrose receptor in water. *Sci. Adv.* **2017**, *3*, e1701126. [[CrossRef](#)] [[PubMed](#)]
77. Hou, Y.; Li, S.; Zhang, Z.; Chen, L.; Zhang, M. A fluorescent platinum(II) metallacycle-cored supramolecular network formed by dynamic covalent bonds and its application in halogen ions and picric acid detection. *Polym. Chem.* **2020**, *11*, 254–258. [[CrossRef](#)]
78. Zhang, M.; Saha, M.L.; Wang, M.; Zhou, Z.; Song, B.; Lu, C.; Yan, X.; Li, X.; Huang, F.; Yin, S.; et al. Multicomponent platinum(II) cages with tunable emission and amino acid sensing. *J. Am. Chem. Soc.* **2017**, *139*, 5067–5074. [[CrossRef](#)] [[PubMed](#)]
79. Domarco, O.; Lötsch, D.; Schreiber, J.; Dinhof, C.; Van Schoonhoven, S.; García, M.D.; Peinador, C.; Keppler, B.K.; Berger, W.; Terenzi, A. Self-assembled Pt₂L₂ boxes strongly bind G-quadruplex DNA and influence gene expression in cancer cells. *Dalton Trans.* **2017**, *46*, 329–332. [[CrossRef](#)]
80. Garci, A.; Castor, K.J.; Fakhoury, J.; Do, J.-L.; Di Trani, J.; Chidchob, P.; Stein, R.S.; Mittermaier, A.K.; Friščić, T.; Sleiman, H. Efficient and rapid mechanochemical assembly of platinum(II) squares for guanine quadruplex targeting. *J. Am. Chem. Soc.* **2017**, *139*, 16913–16922. [[CrossRef](#)]
81. Richards, A.D.; Rodger, A.; Hannon, M.J.; Bolhuis, A. Antimicrobial activity of an iron triple helicate. *Int. J. Antimicrob. Agents* **2009**, *33*, 469–472. [[CrossRef](#)]
82. Howson, S.E.; Bolhuis, A.; Brabec, V.; Clarkson, G.J.; Malina, J.; Rodger, A.; Scott, P. Optically pure, water-stable metallo-helical ‘flexicate’ assemblies with antibiotic activity. *Nat. Chem.* **2012**, *4*, 31–36. [[CrossRef](#)]
83. Wang, H.; Qian, X.; Wang, K.; Su, M.; Haoyang, W.-W.; Jiang, X.; Brzozowski, R.; Wang, M.; Gao, X.; Li, Y.; et al. Supramolecular kandinsky circles with high antibacterial activity. *Nat. Commun.* **2018**, *9*, 1815. [[CrossRef](#)] [[PubMed](#)]
84. Wang, H.; Liu, C.-H.; Wang, K.; Wang, M.; Yu, H.; Kandapal, S.; Brzozowski, R.; Xu, B.; Wang, M.; Lu, S.; et al. Assembling pentatopic terpyridine ligands with three types of coordination moieties into a giant supramolecular hexagonal prism: Synthesis, self-assembly, characterization, and antimicrobial study. *J. Am. Chem. Soc.* **2019**, *141*, 16108–16116. [[CrossRef](#)] [[PubMed](#)]
85. Gao, S.; Yan, X.; Xie, G.; Zhu, M.; Ju, X.; Stang, P.J.; Tian, Y.; Niu, Z. Membrane intercalation-enhanced photodynamic inactivation of bacteria by a metallacycle and TAT-decorated virus coat protein. *Proc. Natl. Acad. Sci. USA* **2019**, *116*, 23437–23443. [[CrossRef](#)] [[PubMed](#)]
86. Bhattacharyya, S.; Ali, S.R.; Venkateswarulu, M.; Howlader, P.; Zangrando, E.; De, M.; Mukherjee, P.S. Self-assembled Pd₁₂ coordination cage as photoregulated oxidase-like nanozyme. *J. Am. Chem. Soc.* **2020**, *142*, 18981–18989. [[CrossRef](#)] [[PubMed](#)]
87. Wu, G.Y.; Shi, X.L.; Phan, H.; Qu, H.; Hu, Y.X.; Yin, G.Q.; Zhao, X.L.; Li, X.P.; Xu, L.; Yu, Q.L.; et al. Efficient self-assembly of heterometallic triangular necklace with strong antibacterial activity. *Nat. Commun.* **2020**, *11*, 1–11. [[CrossRef](#)]

88. Jeyakkumar, P.; Liang, Y.; Guo, M.; Lu, S.; Xu, D.; Li, X.; Guo, B.; He, G.; Chu, D.; Zhang, M. Emissive metallacycle-crosslinked supramolecular networks with tunable crosslinking densities for bacterial imaging and killing. *Angew. Chem. Int. Ed.* **2020**, *59*, 15199–15203. [[CrossRef](#)]
89. Xu, Y.; Tuo, W.; Yang, L.; Sun, Y.; Li, C.; Chen, X.; Yang, W.; Yang, G.; Stang, P.J.; Sun, Y. Design of a metallacycle-based supramolecular photosensitizer for in vivo image-guided photodynamic inactivation of bacteria. *Angew. Chem. Int. Ed.* **2022**, *134*, e202110048.
90. Xu, Y.; Li, C.; Ma, X.; Tuo, W.; Tu, L.; Li, X.; Sun, Y.; Stang, P.J.; Sun, Y. Long wavelength-emissive Ru(II) metallacycle-based photosensitizer assisting in vivo bacterial diagnosis and antibacterial treatment. *Proc. Natl. Acad. Sci. USA* **2022**, *119*, e2209904119. [[CrossRef](#)]
91. Orhan, E.; Garci, A.; Riedel, T.; Soudani, M.; Dyson, P.J.; Therrien, B. Cytotoxic double arene ruthenium metalla-cycles that overcome cisplatin resistance. *J. Organomet. Chem.* **2016**, *803*, 39–44. [[CrossRef](#)]
92. Orhan, E.; Garci, A.; Riedel, T.; Dyson, P.J.; Therrien, B. Cytotoxicity of arene ruthenium metalla-rectangles incorporating bis-pyridyl diimide linkers. *J. Organomet. Chem.* **2016**, *815*, 53–58. [[CrossRef](#)]
93. Gupta, G.; Ogg, G.S.; Nagesh, N.; Bokara, K.K.; Therrien, B. Anticancer activity of large metalla-assemblies built from half-sandwich complexes. *CrystEngComm* **2016**, *18*, 4952–4957. [[CrossRef](#)]
94. Tuo, W.; Xu, Y.; Fan, Y.; Li, J.; Qiu, M.; Xiong, X.; Li, X.; Sun, Y. Biomedical applications of Pt(II) metallacycle/metallacage-based agents: From mono-chemotherapy to versatile imaging contrasts and theranostic platforms. *Coord. Chem. Rev.* **2021**, *443*, 214017. [[CrossRef](#)]
95. Bhowmick, S.; Jana, A.; Singh, K.; Gupta, P.; Gangrade, A.; Mandal, B.B.; Das, N. Coordination-driven self-assembly of ionic irregular hexagonal metallamacrocycles via an organometallic clip and their cytotoxicity potency. *Inorg. Chem.* **2018**, *57*, 3615–3625. [[CrossRef](#)]
96. Jana, A.; Bhowmick, S.; Kumar, S.; Singh, K.; Garg, P.; Das, N. Self-assembly of Pt(II) based nanoscalar ionic hexagons and their anticancer potencies. *Inorg. Chim. Acta* **2019**, *484*, 19–26. [[CrossRef](#)]
97. Datta, S.; Misra, S.K.; Saha, M.L.; Lahiri, N.; Louie, J.; Pan, D.; Stang, P.J. Orthogonal self-assembly of an organoplatinum(II) metallacycle and cucurbit[8]uril that delivers curcumin to cancer cells. *Proc. Natl. Acad. Sci. USA* **2018**, *115*, 8087–8092. [[CrossRef](#)]
98. Ji, T.; Xia, L.; Zheng, W.; Yin, G.-Q.; Yue, T.; Li, X.; Zhang, W.; Zhao, X.-L.; Yang, H.-B. Porphyrin-functionalized coordination star polymers and their potential applications in photodynamic therapy. *Polym. Chem.* **2019**, *10*, 6116–6121. [[CrossRef](#)]
99. Wang, X.; Su, Q.; Zhang, Z.; Yang, J.; Zhang, Y.; Zhang, M. Biotinylated platinum(II) metallacage towards targeted cancer theranostics. *Chem. Commun.* **2020**, *56*, 8460–8463. [[CrossRef](#)]
100. Gupta, G.; Das, A.; Park, K.C.; Tron, A.; Kim, H.; Mun, J.; Mandal, N.; Chi, K.-W.; Lee, C.Y. Self-assembled novel BODIPY-based palladium supramolecules and their cellular localization. *Inorg. Chem.* **2017**, *56*, 4615–4621. [[CrossRef](#)]
101. Gupta, G.; You, Y.; Hadiputra, R.; Jung, J.; Kang, D.-K.; Lee, C.Y. Heterometallic BODIPY-based molecular squares obtained by self-assembly: Synthesis and biological activities. *ACS Omega* **2019**, *4*, 13200–13208. [[CrossRef](#)] [[PubMed](#)]
102. Ajibola Adeyemo, A.; Shettar, A.; Bhat, I.A.; Kondaiah, P.; Mukherjee, P.S. Self-assembly of discrete Ru^{II}₈ molecular cages and their in vitro anticancer activity. *Inorg. Chem.* **2017**, *56*, 608–617. [[CrossRef](#)] [[PubMed](#)]
103. Zhao, Y.; Zhang, L.; Li, X.; Shi, Y.; Ding, R.; Teng, M.; Zhang, P.; Cao, C.; Stang, P.J. Self-assembled ruthenium(II) metallacycles and metallacages with imidazole-based ligands and their in vitro anticancer activity. *Proc. Natl. Acad. Sci. USA* **2019**, *116*, 4090–4098. [[CrossRef](#)] [[PubMed](#)]
104. Yu, G.C.; Zhang, M.M.; Saha, M.L.; Mao, Z.W.; Chen, J.; Yao, Y.; Zhou, Z.J.; Liu, Y.J.; Gao, C.Y.; Huang, F.H.; et al. Antitumor activity of a unique polymer that incorporates a fluorescent self-assembled metallacycle. *J. Am. Chem. Soc.* **2017**, *139*, 15940–15949. [[CrossRef](#)]
105. Zhang, P.; Zhou, Z.; Long, W.; Yan, Y.; Li, Y.; Fu, T.; Liu, Y.; Zhao, Z.; Tan, W.; Stang, P.J. Self-assembled Pt(II) metallacycles enable precise cancer combination chemotherapy. *Proc. Natl. Acad. Sci. USA* **2022**, *119*, e2202255119. [[CrossRef](#)]
106. Zhou, J.; Yu, G.; Yang, J.; Shi, B.; Ye, B.; Wang, M.; Huang, F.; Stang, P.J. Polymeric nanoparticles integrated from discrete organoplatinum(II) metallacycle by stepwise post-assembly polymerization for synergistic cancer therapy. *Chem. Mater.* **2020**, *32*, 4564–4573. [[CrossRef](#)]
107. Sun, Y.; Ding, F.; Zhou, Z.; Li, C.; Pu, M.; Xu, Y.; Zhan, Y.; Lu, X.; Li, H.; Yang, G.; et al. Rhomboidal Pt(II) metallacycle-based NIR-II theranostic nanoprobe for tumor diagnosis and image-guided therapy. *Proc. Natl. Acad. Sci. USA* **2019**, *116*, 1968–1973. [[CrossRef](#)]
108. Zhu, H.; Li, Q.; Shi, B.; Ge, F.; Liu, Y.; Mao, Z.; Zhu, H.; Wang, S.; Yu, G.; Huang, F.; et al. Dual-emissive platinum(II) metallacage with a sensitive oxygen response for imaging of hypoxia and imaging-guided chemotherapy. *Angew. Chem. Int. Ed.* **2020**, *59*, 20208–20214. [[CrossRef](#)]
109. Ding, Y.; Tong, Z.; Jin, L.; Ye, B.; Zhou, J.; Sun, Z.; Yang, H.; Hong, L.; Huang, F.; Wang, W.; et al. An NIR discrete metallacycle constructed from perylene bisimide and tetraphenylethylene fluorophores for imaging-guided cancer radio-chemotherapy. *Adv. Mater.* **2022**, *34*, 2106388. [[CrossRef](#)] [[PubMed](#)]

110. Ma, L.; Yang, T.; Li, S.; Zhang, Z.; Lu, S.; Jeyakkumar, P.; Song, Z.; Li, X.; Yu, G.; Chu, D. Fluorescent metallacycle-cored amphiphilic nanoparticles formed by β -cyclodextrin-based host-guest interactions towards cancer theranostics. *Chem. A Eur. J.* **2020**, *26*, 13031–13038. [[CrossRef](#)]
111. Simões, J.C.S.; Sarpaki, S.; Papadimitroulas, P.; Therrien, B.; Loudos, G. Conjugated photosensitizers for imaging and PDT in cancer research. *J. Med. Chem.* **2020**, *63*, 14119–14150. [[CrossRef](#)] [[PubMed](#)]
112. Gaschard, M.; Nehzat, F.; Cheminel, T.; Therrien, B. Arene ruthenium metalla-assemblies with anthracene moieties for PDT applications. *Inorganics* **2018**, *6*, 97. [[CrossRef](#)]
113. Gallardo-Villagrán, M.; Paulus, L.; Charissoux, J.-L.; Leger, D.Y.; Vergne-Salle, P.; Therrien, B.; Liagre, B. Ruthenium-based assemblies incorporating tetrapyrridylporphyrin panels: A photosensitizer delivery strategy for the treatment of rheumatoid arthritis by photodynamic therapy. *Dalton Trans.* **2022**, *51*, 9673–9680. [[CrossRef](#)] [[PubMed](#)]
114. Yao, Y.; Zhao, R.; Shi, Y.; Cai, Y.; Chen, J.; Sun, S.; Zhang, W.; Tang, R. 2D amphiphilic organoplatinum(II) metallacycles: Their syntheses, self-assembly in water and potential application in photodynamic therapy. *Chem. Commun.* **2018**, *54*, 8068–8071. [[CrossRef](#)] [[PubMed](#)]
115. Zhou, Z.; Liu, J.; Huang, J.; Rees, T.W.; Wang, Y.; Wang, H.; Li, X.; Chao, H.; Stang, P.J. A self-assembled Ru-Pt metallacage as a lysosome-targeting photosensitizer for 2-photon photodynamic therapy. *Proc. Natl. Acad. Sci. USA* **2019**, *116*, 20296–20302. [[CrossRef](#)]
116. Jiang, X.; Zhou, Z.; Yang, H.; Shan, C.; Yu, H.; Wojtas, L.; Zhang, M.; Mao, Z.; Wang, M.; Stang, P.J. Self-assembly of porphyrin-containing metalla-assemblies and cancer photodynamic therapy. *Inorg. Chem.* **2020**, *59*, 7380–7388. [[CrossRef](#)]
117. Li, W.-Y.; Zhao, C.-W.; Zhang, Y.-F.; Guan, Q.; Wan, J.-J.; Ma, J.-P.; Li, Y.-A.; Dong, Y.-B. A metal-organic cage-based nanoagent for enhanced photodynamic antitumor therapy. *Chem. Commun.* **2021**, *57*, 7954–7957. [[CrossRef](#)]
118. Qin, Y.; Chen, L.J.; Dong, F.; Jiang, S.T.; Yin, G.Q.; Li, X.; Tian, Y.; Yang, H.B. Light-controlled generation of singlet oxygen within a discrete dual-stage metallacycle for cancer therapy. *J. Am. Chem. Soc.* **2019**, *141*, 8943–8950. [[CrossRef](#)] [[PubMed](#)]
119. Zhang, J.; Yu, J.; Li, W.; Fan, Y.; Li, Y.; Sun, Y.; Yin, S.; Stang, P.J. A near-infrared BODIPY-based rhomboidal metallacycle for imaging-guided photothermal therapy. *Inorganics* **2022**, *10*, 80. [[CrossRef](#)]
120. Li, G.; Zhang, X.; Zhao, W.; Zhao, W.; Li, F.; Xiao, K.; Yu, Q.; Liu, S.; Zhao, Q. Stable and well-organized near-infrared platinum(II)-acetylide-based metallacycles-mediated cancer phototherapy. *ACS Appl. Mater. Interfaces* **2020**, *12*, 20180–20190. [[CrossRef](#)]
121. Yu, G.; Yu, S.; Saha, M.L.; Zhou, J.; Cook, T.R.; Yung, B.C.; Chen, J.; Mao, Z.; Zhang, F.; Zhou, Z.; et al. A discrete organoplatinum(II) metallacage as a multimodality theranostic platform for cancer photochemotherapy. *Nat. Commun.* **2018**, *9*, 4335. [[CrossRef](#)] [[PubMed](#)]
122. Ding, F.; Chen, Z.; Kim, W.Y.; Sharma, A.; Li, C.; Ouyang, Q.; Zhu, H.; Yang, G.; Sun, Y.; Kim, J.S. A nano-cocktail of an NIR-II emissive fluorophore and organoplatinum(II) metallacycle for efficient cancer imaging and therapy. *Chem. Sci.* **2019**, *10*, 7023–7028. [[CrossRef](#)] [[PubMed](#)]
123. Sun, Y.; Ding, F.; Chen, Z.; Zhang, R.; Li, C.; Xu, Y.; Zhang, Y.; Ni, R.; Li, X.; Yang, G.; et al. Melanin-dot-mediated delivery of metallacycle for NIR-II/photoacoustic dual-modal imaging-guided chemo-photothermal synergistic therapy. *Proc. Natl. Acad. Sci. USA* **2019**, *116*, 16729–16735. [[CrossRef](#)]
124. Acharyya, K.; Bhattacharyya, S.; Sepehrpour, H.; Chakraborty, S.; Lu, S.; Shi, B.; Li, X.; Mukherjee, P.S.; Stang, P.J. Self-assembled fluorescent Pt(II) metallacycles as artificial light-harvesting systems. *J. Am. Chem. Soc.* **2019**, *141*, 14565–14569. [[CrossRef](#)]
125. Zhu, J.L.; Xu, L.; Ren, Y.Y.; Zhang, Y.; Liu, X.; Yin, G.Q.; Sun, B.; Cao, X.; Chen, Z.; Zhao, X.L.; et al. Switchable organoplatinum metallacycles with high quantum yields and tunable fluorescence wavelengths. *Nat. Commun.* **2019**, *10*, 4285. [[CrossRef](#)]
126. He, Z.; Li, M.; Que, W.; Stang, P.J. Self-assembly of metal-ion-responsive supramolecular coordination complexes and their photophysical properties. *Dalton Trans.* **2017**, *46*, 3120–3124. [[CrossRef](#)]
127. Zhang, C.-W.; Ou, B.; Jiang, S.-T.; Yin, G.-Q.; Chen, L.-J.; Xu, L.; Li, X.; Yang, H.-B. Cross-linked AIE supramolecular polymer gels with multiple stimuli-responsive behaviours constructed by hierarchical self-assembly. *Polym. Chem.* **2018**, *9*, 2021–2030. [[CrossRef](#)]
128. Zhang, D.; Ronson, T.K.; Güryel, S.; Thoburn, J.D.; Wales, D.J.; Nitschke, J.R. Temperature controls guest uptake and release from Zn_4L_4 tetrahedra. *J. Am. Chem. Soc.* **2019**, *141*, 14534–14538. [[CrossRef](#)] [[PubMed](#)]
129. Nguyen, B.T.; Grommet, A.B.; Tron, A.; Georges, M.C.A.; Nitschke, J.R. Heat engine drives transport of an $Fe(II)_4L_4$ cage and cargo. *Adv. Mater.* **2020**, *32*, e1907241. [[CrossRef](#)] [[PubMed](#)]
130. Tang, J.H.; Sun, Y.; Gong, Z.L.; Li, Z.Y.; Zhou, Z.X.; Wang, H.; Li, X.P.; Saha, M.L.; Zhong, Y.W.; Stang, P.J. Temperature-responsive fluorescent organoplatinum(II) metallacycles. *J. Am. Chem. Soc.* **2018**, *140*, 7723–7729. [[CrossRef](#)]
131. Lewis, J.E.M.; Gavey, E.L.; Cameron, S.A.; Crowley, J.D. Stimuli-responsive Pd_2L_4 metallosupramolecular cages: Towards targeted cisplatin drug delivery. *Chem. Sci.* **2012**, *3*, 778–784. [[CrossRef](#)]
132. Sun, Y.; Chen, C.; Zhang, F.; Jiang, S.; Stang, P.J. Pt Metallacage-based centimeter films for smart emissive poly(N-isopropylacrylamide) hydrogel devices. *Mater. Chem. Phys.* **2022**, *277*, 125544. [[CrossRef](#)]

133. Gu, Y.; Alt, E.A.; Wang, H.; Li, X.; Willard, A.P.; Johnson, J.A. Photoswitching topology in polymer networks with metal-organic cages as crosslinks. *Nature* **2018**, *560*, 65–69. [[CrossRef](#)] [[PubMed](#)]
134. Shi, B.; Qin, P.; Chai, Y.; Qu, W.-J.; Shangguan, L.; Lin, Q.; Zhang, Y.-M.; Sun, Y.; Huang, F.; Stang, P.J. An organoplatinum(II) metallacycle-based supramolecular amphiphile and its application in enzyme-responsive controlled release. *Inorg. Chem.* **2022**, *61*, 8090–8095. [[CrossRef](#)] [[PubMed](#)]

Disclaimer/Publisher's Note: The statements, opinions and data contained in all publications are solely those of the individual author(s) and contributor(s) and not of MDPI and/or the editor(s). MDPI and/or the editor(s) disclaim responsibility for any injury to people or property resulting from any ideas, methods, instructions or products referred to in the content.